

Fate of the topological susceptibility in two-color dense QCD

Mamiya Kawaguchi,^a Daiki Suenaga^{b,c}

^a*School of Nuclear Science and Technology, University of Chinese Academy of Sciences, Beijing 100049, China*

^b*Few-Body Systems in Physics Laboratory, RIKEN Nishina Center, Wako 351-0198, Japan*

^c*Research Center for Nuclear Physics, Osaka University, Ibaraki 567-0048, Japan*

E-mail: mamiya@ucas.ac.cn, daiki.suenaga@riken.jp

ABSTRACT: We explore the topological susceptibility at finite quark chemical potential and zero temperature in two-color QCD (QC₂D) with two flavors. Through the Ward-Takahashi identities of QC₂D, we find that the topological susceptibility in the vacuum solely depends on three observables: the pion decay constant, the pion mass, and the η mass in the low-energy regime of QC₂D. Based on the identities, we numerically evaluate the topological susceptibility at finite quark chemical potential using the linear sigma model with the approximate Pauli-Gursey $SU(4)$ symmetry. Our findings indicate that, in the absence of $U(1)_A$ anomaly effects represented by the Kobayashi-Maskawa-'t Hooft-type determinant interaction, the topological susceptibility vanishes in both the hadronic and baryon superfluid phases. On the other hand, when the $U(1)_A$ anomaly effects are present, the constant and nonzero topological susceptibility is induced in the hadronic phase, reflecting the mass difference between the pion and η meson. Meanwhile, in the superfluid phase it begins to decrease smoothly. The asymptotic behavior of the decrement is fitted by the continuous reduction of the chiral condensate in dense QC₂D, which is similar to the behavior observed in hot three-color QCD matter. In addition, effects from the finite diquark source on the topological susceptibility are discussed. We expect that the present study provides a clue to shed light on the role of the $U(1)_A$ anomaly in cold and dense QCD matter.

Contents

1	Introduction	1
2	Topological susceptibility based on Ward-Takahashi identities of QC_2D	4
3	Low-energy effective-model description of two-flavor QC_2D	8
4	Topological susceptibility at low energy	11
4.1	Matching between low-energy effective model and underlying QC_2D	11
4.2	Topological susceptibility across baryon superfluid phase transition	13
5	Fate of topological susceptibility in dense QC_2D	15
5.1	$U(1)_A$ anomaly contribution and μ_q dependence of topological susceptibility	16
5.2	Asymptotic behavior of topological susceptibility in dense baryonic matter	20
6	Contamination by diquark source field	21
6.1	Diquark source effect on topological susceptibility	21
6.2	Diquark source effect on μ_q dependence of topological susceptibility	24
7	Summary and discussion	26
A	Partner structures of the susceptibility functions	28
B	Derivation of WTIs (2.12) and (6.8)	30
C	Alternative expression of the topological susceptibility	31

1 Introduction

In Quantum Chromodynamics (QCD), the $U(1)_A$ anomaly, i.e., the non-conservation of the $U(1)_A$ axial current caused by the gluonic quantum corrections, plays crucial roles in the low-energy physics governed by the spontaneous breaking of the chiral symmetry. For instance, the $U(1)_A$ anomaly affects the hadron mass spectrum to yield the heavy η' meson [1] and the order of the chiral phase transition in QCD matter [2]. In addition to these low-energy aspects, the $U(1)_A$ anomaly is also closely related with topological vacuum structures of QCD [3], which is described by the anomalous gluonic operator tagged with the θ parameter. The characteristics of the θ -dependent QCD vacuum is captured by the *topological susceptibility*: the curvature of the QCD effective potential with respect to θ .

The symmetry breakings in QCD are reflected in meson susceptibility functions defined by two-point functions of quark composite operators in the low-energy limit. At the

hadronic level, the so-called *chiral-partner structure* would be an indication of this property [4]. That is, at high temperature and/or density where chiral symmetry tends to be restored, masses of the mesons related by the chiral transformation become degenerate, and so do the corresponding meson susceptibility functions. This implies that, indeed, the meson susceptibility functions can be regarded as alternative probes to measure the strength of chiral symmetry breaking and restoration. In a similar way, the effective restoration of $U(1)_A$ symmetry can be quantified by the degeneracies of the meson susceptibility functions connected by the $U(1)_A$ transformation.

Making use of the Ward-Takahashi identity (WTI) associated with chiral symmetry, one can show that the topological susceptibility is also correlated with the chiral- and $U(1)_A$ -partner structures in the meson susceptibility functions [5–9]. Thereby, the topological susceptibility can also be referred to as the indicator for the breaking strength of $U(1)_A$ symmetry through the chiral phase transition. In fact, lattice QCD simulations at the physical quark masses support that the magnitude of the topological susceptibility smoothly decreases at high temperatures [10–12]. Furthermore, a strong correlation with the chiral restoration has also been studied through the meson susceptibility functions within 2 flavor QCD [13–17] and 2 + 1 flavor QCD [18–20].

Thus far, the susceptibilities in hot QCD matter have been explored by both lattice simulations [10–20] and effective model analyses [7, 8, 21] in order to gain deeper insights into the symmetry properties of QCD in the extreme environment. However, at finite quark chemical potential μ_q lattice QCD simulations with three colors suffer from the *sign problem*, and then the first-principle numerical computations cannot apply in baryonic matter straightforwardly [22]. For this reason, our understanding of QCD at low-temperature and high-density regime is still limited compared to that in hot medium.

In light of the difficulty of three-color QCD on lattice simulations with finite μ_q , two-color QCD (QC₂D) with two flavors provides us with a valuable testing ground. This is because the sign problem is resolved in such QCD-like theory owing to its pseudo-real property [23]. Focusing on this fact, many efforts from lattice simulations are being devoted to understandings of, e.g., phase structures, thermodynamics quantities, electromagnetic responses, the hadron mass spectrum, and gluon propagators in cold and dense QC₂D matter [24–49]. In association with such numerical examinations, theoretical investigations of QC₂D at finite μ_q based on effective models have been done [50–65].

In QC₂D, diquarks composed of two quarks are treated as color-singlet baryons. In other words, baryons exhibit bosonic behavior similarly to mesons. Reflecting this fact in QC₂D, $SU(2)_L \times SU(2)_R$ chiral symmetry is extended to the so-called Pauli-Gursey $SU(4)$ symmetry, which allows us to describe diquark baryons and light mesons in the single multiplets. Accordingly, the spontaneously symmetry-breaking pattern caused by the chiral condensate is changed to $SU(4) \rightarrow Sp(4)$ [50, 51]. Despite such an extension of chiral symmetry, symmetry structures of the $U(1)_A$ axial anomaly induced by gluonic configurations essentially do not differ from those in ordinary three-color QCD.

To shed light on the role of the $U(1)_A$ axial anomaly in baryonic QCD matter, the μ_q dependence of the topological susceptibility has been numerically measured by lattice numerical simulations of QC₂D [30, 33, 41, 45]. The recent lattice result in Ref. [41]

indicates that the effect of μ_q does not exert any influence on the behavior of the topological susceptibility in baryonic matter, resulting in an approximately constant value. In contrast, the other group shows that the topological susceptibility is suppressed in high-density regions [45]. Hence, there exist discrepancies among the lattice simulations at finite quark chemical potentials, and the fate of topological susceptibility at high-density regions is still controversial.

In this paper, motivated by the above puzzle, we investigate the topological susceptibility in zero-temperature QC₂D at finite μ_q based on an effective-model approach. In particular, we employ the linear sigma model based on the approximate Pauli-Gursey $SU(4)$ symmetry invented in Ref. [65]. Notably, this model is capable of treating the η meson which plays a significant role in describing the $U(1)_A$ anomaly structures consistently with other light mesons and diquark baryons. In QC₂D, since the diquarks obey the Bose-Einstein statistics, when the mass of the ground-state diquark becomes zero they begin to exhibit the Bose-Einstein condensates (BECs), leading to the emergence of the *diquark condensed phase* [50, 51]. This phase is also referred to as the *baryon superfluid phase* due to the violation of $U(1)_B$ baryon-number symmetry. Meanwhile, the stable phase with no such BECs connected to the vacuum, i.e., zero temperature and zero chemical potential, is called the *hadronic phase*. The former nontrivial phase triggers a rich hadron mass spectrum such as a mixing among hadrons sharing the identical quantum numbers except for the baryon number.

Within the linear sigma model, the influences of the $U(1)_A$ anomaly on hadrons are described by the so-called Kobayashi-Maskawa-'t Hooft (KMT)-type determinant interaction [66–69], which only breaks $U(1)_A$ symmetry but preserves the Pauli-Gursey $SU(4)$ one. This interaction induces a mass difference between the pion and η meson in the vacuum. Thus, in the present analysis we particularly focus on the strength of the KMT-type interaction, in other words, the mass difference between the pion and η meson, in order to quantify roles of the $U(1)_A$ anomaly in the topological susceptibility. Besides, in lattice simulations source contributions with respect to the diquark condensate would be left sizable, so in this paper we also investigate the diquark source effects so as to facilitate the comparison with lattice data.

This paper is organized as follows. In Sec. 2 we present general properties associated with the topological susceptibility in QC₂D by focusing on the underlying QC₂D theory, and discuss symmetry partner structures of the meson susceptibility functions. In Sec. 3, the emergence of the Pauli-Gursey $SU(4)$ symmetry in QC₂D is briefly explained, and our linear sigma model regarded as a low-energy theory of QC₂D is introduced. In Sec. 4 we show how the topological susceptibility within the linear sigma model is evaluated by explicitly demonstrating the matching between underlying QC₂D and the linear sigma model. Based on it, in Sec. 5 we show our numerical results on the topological susceptibility at finite μ_q . In order to facilitate the comparison with lattice simulations, in Sec. 6 we also exhibit the results in the presence of the diquark source contributions. Finally, in Sec. 7 we conclude our present study.

2 Topological susceptibility based on Ward-Takahashi identities of QC₂D

Our main aim of this paper is to reveal properties of the topological susceptibility in zero-temperature QC₂D with finite quark chemical potential μ_q . In this section, we present an analytic formula of the topological susceptibility based on the underlying QC₂D Lagrangian [5–9], which is useful for the investigation within the effective-model framework of the linear sigma model.

The topological susceptibility is one of indicators to measure the magnitude of the $U(1)_A$ anomaly, which is related to nontrivial gluonic configurations such as the instantons [3]. Hence, we need to return to QCD Lagrangian where such microscopic degrees of freedom are treated manifestly. In two-flavor QC₂D, the Lagrangian including the so-called QCD θ -term in Minkowski spacetime is of the form

$$\mathcal{L}_{\text{QC}_2\text{D}} = \bar{\psi}(i\gamma^\mu D_\mu - m_l)\psi - \frac{1}{4}G_{\mu\nu}^a G^{\mu\nu,a} + \theta \frac{g^2}{64\pi^2} \epsilon^{\mu\nu\rho\sigma} G_{\mu\nu}^a G_{\rho\sigma}^a. \quad (2.1)$$

As for the first term, $\psi = (u, d)^T$ denotes the two-flavor quark doublet and $D_\mu\psi = (\partial_\mu - i\mu_q\delta_{\mu 0} - igA_\mu^a T_c^a)\psi$ is the covariant derivative incorporating effects from a quark chemical potential μ_q and interactions with a gluon field A_μ^a . The 2×2 matrix $T_c^a = \tau_c^a/2$ is the generator of $SU(2)_c$ color group with τ_c^a being the Pauli matrix. Besides, g and m_l are the QCD coupling constant and a current quark mass where the isospin symmetric limit is taken, $m_u = m_d \equiv m_l$. The second term in Eq. (2.1) is a gluon kinetic term where $G_{\mu\nu}^a = \partial_\mu A_\nu^a - \partial_\nu A_\mu^a + g\epsilon^{abc}A_\mu^b A_\nu^c$ is the field strength of gluons. The last ingredient of QC₂D Lagrangian in Eq. (2.1) is the θ -term of QC₂D, which is described by a flavor-singlet topological operator $Q \equiv (g^2/64\pi^2)\epsilon^{\mu\nu\rho\sigma} G_{\mu\nu}^a G_{\rho\sigma}^a$ tagged with the θ -parameter. Our purpose in this subsection is to derive useful identities with respect to the topological susceptibility, so that only the θ -dependent term in Eq. (2.1), which is gauge invariant, plays significant roles. For this reason, the gauge-fixing terms and the corresponding Faddeev-Popov determinant, which do not affect the following discussions, have been omitted in Eq. (2.1).

The generating functional of $\mathcal{L}_{\text{QC}_2\text{D}}$ in the path-integral formulation is given by

$$Z_{\text{QC}_2\text{D}} = \int [d\bar{\psi}d\psi][dA] \exp \left[i \int d^4x \mathcal{L}_{\text{QC}_2\text{D}} \right], \quad (2.2)$$

and the θ -dependent effective action of QC₂D is evaluated as

$$\Gamma_{\text{QC}_2\text{D}} = -i \ln Z_{\text{QC}_2\text{D}}. \quad (2.3)$$

The topological susceptibility χ_{top} is defined by the curvature of $\Gamma_{\text{QC}_2\text{D}}$, i.e., a second derivative with respect to θ at $\theta = 0$:

$$\chi_{\text{top}} = - \int d^4x \frac{\delta^2 \Gamma_{\text{QC}_2\text{D}}}{\delta\theta(x)\delta\theta(0)} \Big|_{\theta=0}. \quad (2.4)$$

Thus, from a straightforward calculation of Eq. (2.4) based on the QC₂D Lagrangian in Eq. (2.1), one can find that the topological susceptibility is described by a two-point

correlation function of the topological operator $Q = (g^2/64\pi^2)\epsilon^{\mu\nu\rho\sigma}G_{\mu\nu}^a G_{\rho\sigma}^a$:

$$\chi_{\text{top}} = -i \int d^4x \langle 0|TQ(x)Q(0)|0\rangle, \quad (2.5)$$

with T denoting the time ordered product. It should be noted that contributions stemming from a product of $\langle Q \rangle$ have been omitted from Eq. (2.5) due to the parity conservation. The topological susceptibility in Eq. (2.5) is written in terms of the gluonic operator Q , which would not be a manageable expression since our task in this paper is to evaluate χ_{top} from a low-energy effective model involving only hadronic degrees of freedom. Difficulties in matching the susceptibility from the effective models with that from underlying QC₂D are, however, remedied by utilizing the $U(1)_A$ axial rotation properly as demonstrated below.

Under the $U(1)_A$ rotation with a rotation angle α_A , the quark doublet transforms as

$$\psi \rightarrow \exp(i\alpha_A/2 \gamma_5)\psi. \quad (2.6)$$

Meanwhile, within the path-integral formalism the gluonic quantum anomaly is generated by the fermionic measure $[d\bar{\psi}d\psi]$ according to the Fujikawa's method [70], resulting in that the rotated generating functional reads

$$\begin{aligned} Z_{\text{QC}_2\text{D}} \rightarrow \int [d\bar{\psi}d\psi][dA] \exp \left[i \int d^4x \left(\bar{\psi}i\gamma^\mu D_\mu\psi - m_l\bar{\psi} \exp(i\alpha_A\gamma_5)\psi \right. \right. \\ \left. \left. - \frac{1}{4}G_{\mu\nu}^a G^{\mu\nu,a} + (\theta - 2\alpha_A) \frac{g^2}{64\pi^2} \epsilon^{\mu\nu\rho\sigma} G_{\mu\nu}^a G_{\rho\sigma}^a \right) \right]. \end{aligned} \quad (2.7)$$

Thus, when choosing the rotation angle to be $\alpha_A = \theta/2$, the θ -dependence of the QCD θ -term is transferred into the quark mass term as

$$Z_{\text{QC}_2\text{D}} = \int [d\bar{\psi}d\psi][dA] \exp \left[i \int d^4x \left(\bar{\psi}i\gamma^\mu D_\mu\psi - m_l\bar{\psi} \exp(i\theta/2 \gamma_5)\psi - \frac{1}{4}G_{\mu\nu}^a G^{\mu\nu,a} \right) \right]. \quad (2.8)$$

Following the procedure in Eqs. (2.3) and (2.4) with the rotated generating functional (2.8), the topological susceptibility χ_{top} is now expressed by fermionic operators as

$$\chi_{\text{top}} = -\frac{1}{4} [m_l \langle \bar{\psi}\psi \rangle + im_l^2 \chi_\eta], \quad (2.9)$$

where $\langle \bar{\psi}\psi \rangle$ is the chiral condensate serving as an order parameter of the spontaneous chiral-symmetry breaking, and χ_η denotes an η -meson susceptibility function defined by

$$\chi_\eta = \int d^4x \langle 0|T(i\bar{\psi}\gamma_5\psi)(x)(i\bar{\psi}\gamma_5\psi)(0)|0\rangle. \quad (2.10)$$

It should be noted that, from the rotated generating functional in Eq. (2.7), a non-conservation law of the $U(1)_A$ axial current $j_A^\mu = \bar{\psi}\gamma^\mu\gamma_5\psi$ is also obtained as

$$\partial_\mu j_A^\mu = 2m_l\bar{\psi}i\gamma_5\psi + \frac{g^2}{16\pi^2} \epsilon^{\mu\nu\rho\sigma} G_{\mu\nu}^a G_{\rho\sigma}^a. \quad (2.11)$$

The topological susceptibility (2.9) is further reduced to a handleable form. In fact, using the $SU(2)_L \times SU(2)_R$ chiral-partner relation shown in Appendix A, a chiral WTI with respect to the chiral condensate $\langle \bar{\psi}\psi \rangle$ is derived as in Appendix B, which reads

$$\langle \bar{\psi}\psi \rangle = -im_l \chi_\pi . \quad (2.12)$$

In this identity, χ_π is a pion susceptibility function defined by

$$\chi_\pi \delta^{ab} = \int d^4x \langle 0 | T(i\bar{\psi}\gamma_5 \tau_f^a \psi)(x) (i\bar{\psi}\gamma_5 \tau_f^b \psi)(0) | 0 \rangle , \quad (2.13)$$

with τ_f^a being the Pauli matrix in the flavor space. Therefore, inserting Eq. (2.12) into Eq. (2.9), the topological susceptibility is found to be determined in terms of a difference of χ_π and χ_η as

$$\chi_{\text{top}} = \frac{im_l^2}{4} (\chi_\pi - \chi_\eta) . \quad (2.14)$$

This expression is identical to the one obtained in ordinary three-color QCD through the WTI [5–9]. Here, to facilitate an understanding of the role of topological susceptibility, we insert the scalar meson susceptibilities χ_σ and χ_{a_0} in Eq. (2.14):

$$\begin{aligned} \chi_{\text{top}} &= \frac{im_l^2}{4} [(\chi_\pi - \chi_\sigma) - (\chi_\eta - \chi_\sigma)] , \\ \chi_{\text{top}} &= \frac{im_l^2}{4} [(\chi_\pi - \chi_{a_0}) - (\chi_\eta - \chi_{a_0})] , \end{aligned} \quad (2.15)$$

where χ_σ and χ_{a_0} are the susceptibility functions made of the composite operators $\bar{\psi}\psi$ and $\bar{\psi}\tau_f^a\psi$, respectively. Indeed, under the chiral $SU(2)_L \times SU(2)_R$ rotation and the $U(1)_A$ rotation, the meson susceptibility functions are transformed into each other:

$$\begin{array}{ccc} \chi_\pi & \xleftrightarrow{SU(2)} & \chi_\sigma \\ U(1)_A \updownarrow & & \updownarrow U(1)_A \\ \chi_{a_0} & \xleftrightarrow{SU(2)} & \chi_\eta \end{array}$$

as explicitly shown in Appendix A. With this transformation, one can realize that the topological susceptibility in Eq. (2.15) is described by the combinations of the chiral $SU(2)$ partner $\chi_\pi \leftrightarrow \chi_\sigma$ ($\chi_{a_0} \leftrightarrow \chi_\eta$) and the $U(1)$ axial partner $\chi_\pi \leftrightarrow \chi_{a_0}$ ($\chi_\sigma \leftrightarrow \chi_\eta$). When chiral symmetry is restored and the order parameter of the spontaneous chiral symmetry breaking vanishes $\langle \bar{\psi}\psi \rangle \rightarrow 0$, the chiral partner becomes (approximately) degenerate:

$$SU(2)_L \times SU(2)_R \text{ restoration limit : } \begin{cases} \chi_\pi - \chi_\sigma \rightarrow 0 \\ \chi_{a_0} - \chi_\eta \rightarrow 0 \end{cases} . \quad (2.16)$$

After the chiral restoration, the topological susceptibility is dominated by the $U(1)_A$ axial partner: $\chi_{\text{top}} \sim \chi_\eta - \chi_\sigma$ ($\chi_{\text{top}} \sim \chi_\pi - \chi_{a_0}$), so that χ_{top} acts as the indicator for the

breaking strength of $U(1)_A$ symmetry. It should be noted that χ_{top} trivially vanishes in the chiral limit ($m_l = 0$) as seen from Eq. (2.14). In this limit, the topological susceptibility is no longer regarded as the indicator. This can also be understood by the fact that when $m_l = 0$, the θ dependence of the generating functional in Eq. (2.8) disappears, resulting in the vanishing topological susceptibility defined by a second derivative with respect to θ .

When studying with a low-energy effective model, the analytical expression of (2.14) is useful for evaluating the topological susceptibility χ_{top} . Here, we show another expression of χ_{top} so as to see contributions from the chiral condensate $\langle\bar{\psi}\psi\rangle$ clearly. That is, from the identity (2.12) one can rewrite Eq. (2.14) into

$$\chi_{\text{top}} = -\frac{m_l\langle\bar{\psi}\psi\rangle}{4}\delta_m. \quad (2.17)$$

In this expression, the dimensionless quantity δ_m is defined by

$$\delta_m \equiv 1 - \frac{\chi_\eta}{\chi_\pi}, \quad (2.18)$$

which measures the variation of the susceptibility functions χ_π and χ_η . Equation (2.17) indicates, indeed, that the topological susceptibility is proportional to the chiral condensate $\langle\bar{\psi}\psi\rangle$ and δ_m ; the explicit chiral-symmetry breaking is entangled with the $U(1)_A$ anomaly contribution captured by the quantity δ_m in χ_{top} . This structure plays an important role in determining the asymptotic behavior of χ_{top} at sufficiently large μ_q where chiral symmetry is restored.

Furthermore, the Gell-Mann-Oakes-Renner (GOR) relation: $f_\pi^2 m_\pi^2 = -m_l\langle\bar{\psi}\psi\rangle/2$ [71], enables us to rewrite the topological susceptibility in Eq. (2.17) as

$$\chi_{\text{top}} = \frac{f_\pi^2 m_\pi^2}{2}\delta_m, \quad (2.19)$$

where f_π is the pion decay constant and m_π is the pion mass. It is obvious from its derivation that Eq. (2.19) holds model-independently.^{#1} Notably, the quantity δ_m in the vacuum is solely determined by the masses of pion and η meson as

$$\delta_m \rightarrow 1 - \frac{m_\pi^2}{m_\eta^2}, \quad (2.20)$$

as long as we stick to the low-energy regime of QC₂D where $\chi_\pi \sim -i/m_\pi^2$ and $\chi_\eta \sim -i/m_\eta^2$ can apply. Therefore, Eq. (2.19) implies that the topological susceptibility in the vacuum is expressed by three basic observables in low-energy QC₂D: f_π , m_π and m_η . We note that $\delta_m \rightarrow 1$ corresponds to the significantly large anomaly effects, while $\delta_m \rightarrow 0$ implies no such effects. We also note that Leutwyler and Smilga obtained the following form based on the Chiral Perturbation Theory (ChPT) in three-color QCD [72]:

$$\chi_{\text{top}}^{(\text{LS})} = -\frac{m_l\langle\bar{\psi}\psi\rangle}{4} = \frac{f_\pi^2 m_\pi^2}{2}, \quad (2.21)$$

^{#1}The GOR relation $f_\pi^2 m_\pi^2 = -m_l\langle\bar{\psi}\psi\rangle/2$ is derived model-independently but with an assumption that the two-point function of the pseudoscalar channel $D_\pi^{\delta ab} \equiv \int d^4x \langle 0|T(i\bar{\psi}\gamma_5\tau_f^a\psi)(x)(i\bar{\psi}\gamma_5\tau_f^b\psi)(0)|0\rangle e^{-ip\cdot x}$ is dominated by the lightest pseudoscalar-meson pole: $D_\pi \propto i/(p^2 - m_\pi^2)$, as in the case of three-color QCD. Accordingly, the relation (2.19) also holds upon the pole dominance of the lightest pseudoscalar meson.

where the χ_η contributions are missing. Indeed, in Eq. (2.21), the large anomaly is accidentally taken into account: $\delta_m = 1$. Even in the case of QC₂D, the Leutwyler-Smilga relation was also found in [73].

3 Low-energy effective-model description of two-flavor QC₂D

In QC₂D, diquarks (antidiquarks) carrying the quark number +2 (−2) are treated as color-singlet baryons, namely, baryons become bosonic similarly to mesons. Accordingly, the so-called Pauli-Gursey $SU(4)$ symmetry, which enables us to treat both the baryons and mesons in a consistent way, emerges [50, 51]. In this section, we briefly explain how the Pauli-Gursey $SU(4)$ symmetry manifests itself from QC₂D Lagrangian, and based on the symmetry we present the linear sigma model which describes couplings among the baryons and mesons.

Thanks to pseudoreal properties of the $SU(2)$ generators for color and Dirac spaces, $T_c^a = -\tau^2(T_c^a)^T\tau^2$ and $\sigma^i = -\sigma^2(\sigma^i)^T\sigma^2$ (σ^i is the Pauli matrix in the Dirac space), one can show that the kinetic term of quarks coupling with gauge fields in QC₂D, i.e., the first piece in Eq. (2.1), is rewritten to

$$\mathcal{L}_{\text{QC}_2\text{D}}^{(\text{kin})} = \Psi^\dagger i\sigma^\mu D_\mu \Psi , \quad (3.1)$$

with $\sigma^\mu = (\mathbf{1}, \sigma^i)$, in the Weyl representation. In Eq. (3.1) the quark field Ψ is given by a four-component column vector in the flavor space as

$$\Psi = \begin{pmatrix} \psi_R \\ \tilde{\psi}_L \end{pmatrix} = \begin{pmatrix} u_R \\ d_R \\ \tilde{u}_L \\ \tilde{d}_L \end{pmatrix} , \quad (3.2)$$

where $\psi_{L(R)} = \frac{1 \mp \gamma_5}{2} \psi$ denotes the left-handed (right-handed) quark field and $\tilde{\psi}_{L(R)}$ is the conjugate one:

$$\tilde{\psi}_{L(R)} = \sigma^2 \tau_c^2 \psi_{L(R)}^* . \quad (3.3)$$

Equation (3.1) implies that the quark kinetic term in QC₂D is invariant under an $SU(4)$ transformation for the quark field as

$$\Psi \rightarrow g\Psi , \quad (3.4)$$

with $g \in SU(4)$. Thus, it is proven that $SU(2)_L \times SU(2)_R$ chiral symmetry in QC₂D is extended to the $SU(4)$ one which is often referred to as the Pauli-Gursey $SU(4)$ symmetry [50, 51].

Similarly to the kinetic part, the quark mass term, i.e., the second piece in Eq. (2.1), is also expressed in terms of the four-component field Ψ , which reads

$$\mathcal{L}_{\text{QC}_2\text{D}}^{(\text{mass})} = \frac{m_l}{2} \left(\Psi^T \sigma^2 \tau_c^2 E \Psi + \Psi^\dagger \sigma^2 \tau_c^2 E^T \Psi^* \right) . \quad (3.5)$$

This term, however, breaks the Pauli-Gursey $SU(4)$ symmetry explicitly due to the presence of a symplectic matrix in the flavor space

$$E = \begin{pmatrix} 0 & \mathbf{1} \\ -\mathbf{1} & 0 \end{pmatrix}, \quad (3.6)$$

in between the two quark fields. For this reason, the systematic treatment based on the viewpoint of the $SU(4)$ symmetry is spoiled by the quark masses. To recover the systematics, we introduce a spurion field ζ_{sp} which transforms as

$$\zeta_{\text{sp}} \rightarrow g \zeta_{\text{sp}} g^T. \quad (3.7)$$

To construct the $SU(4)$ -invariant Lagrangian, the quark mass term is promoted to the spurion term

$$\mathcal{L}_{\text{QC}_2\text{D}}^{(\text{sp})} = -\Psi^T \sigma^2 \tau_c^2 \zeta_{\text{sp}}^\dagger \Psi - \Psi^\dagger \sigma^2 \tau_c^2 \zeta_{\text{sp}} \Psi^*. \quad (3.8)$$

In fact, one can show that the quark mass term (3.5) is appropriately reproduced by taking the vacuum expectation value (VEV) of the spurion field as

$$\langle \zeta_{\text{sp}} \rangle = \frac{m_l}{2} E. \quad (3.9)$$

In what follows, we construct the linear sigma model to describe hadrons at the low-energy regime of QC_2D , based on the symmetries explained above. The fundamental building block of the linear sigma model in QC_2D is a 4×4 matrix field Σ_{ij} whose symmetry properties are the same as those of a quark bilinear field $\Psi_j^T \sigma^2 \tau_c^2 \Psi_i$. That is, Σ transforms as

$$\Sigma \rightarrow g \Sigma g^T, \quad (3.10)$$

under the $SU(4)$ transformation. As explained in Ref. [65] in detail, the Σ can be parameterized by low-lying hadrons in QC_2D as

$$\Sigma = (S^a - iP^a)X^a E + (B'^i - iB^i)X^i E, \quad (3.11)$$

where S^a , P^a , B^i and B'^i represent scalar mesons, pseudoscalar mesons, positive-parity diquark baryons and negative-parity diquark baryons, respectively. The 4×4 matrices X^a and X^i are generators of $U(4)$ defined by

$$\begin{aligned} X^a &= \frac{1}{2\sqrt{2}} \begin{pmatrix} \tau_f^a & 0 \\ 0 & (\tau_f^a)^T \end{pmatrix} \quad (a = 0, 1, 2, 3), \\ X^i &= \frac{1}{2\sqrt{2}} \begin{pmatrix} 0 & D_f^i \\ (D_f^i)^\dagger & 0 \end{pmatrix} \quad (i = 4, 5), \end{aligned} \quad (3.12)$$

where $\tau_f^0 = \mathbf{1}_{2 \times 2}$ in the flavor space, and D_f^i represent $D_f^4 = \tau_f^2$ and $D_f^5 = i\tau_f^2$. Following the parametrization given in Ref. [65], we employ the following hadron assignment for Σ :

$$\Sigma = \frac{1}{2} \begin{pmatrix} 0 & -B' + iB & \frac{\sigma - i\eta + a^0 - i\pi^0}{\sqrt{2}} & a^+ - i\pi^+ \\ B' - iB & 0 & a^- - i\pi^- & \frac{\sigma - i\eta - a^0 + i\pi^0}{\sqrt{2}} \\ -\frac{\sigma - i\eta + a^0 - i\pi^0}{\sqrt{2}} & -a^- + i\pi^- & 0 & -\bar{B}' + i\bar{B} \\ -a^+ + i\pi^+ & -\frac{\sigma - i\eta - a^0 + i\pi^0}{\sqrt{2}} & \bar{B}' - i\bar{B} & 0 \end{pmatrix}, \quad (3.13)$$

where $\pi^0 = P^3$ and $\pi^\pm = (P^1 \mp iP^2)/\sqrt{2}$ are the pions, $\eta = P^0$ is the η meson, $\sigma = S^0$ is the iso-singlet scalar meson (σ meson), $a_0^0 = S^3$ and $a_0^\pm = (S^1 \mp iS^2)/\sqrt{2}$ are the iso-triplet scalar mesons (a_0 mesons), $B = (B^5 - iB^4)/\sqrt{2}$ [$\bar{B} = (B^5 + iB^4)/\sqrt{2}$] is the positive-parity diquark baryon (the antidiquark baryon), and $B' = (B'^5 - iB'^4)/\sqrt{2}$ [$\bar{B}' = (B'^5 + iB'^4)/\sqrt{2}$] is the negative-parity diquark baryon (the antidiquark baryon).

With the matrix Σ given in Eq. (3.13), our linear sigma model in QC₂D which respects the Pauli-Gursey $SU(4)$ symmetry is obtained as

$$\mathcal{L}_{\text{LSM}} = \text{tr}[D_\mu \Sigma^\dagger D^\mu \Sigma] - V, \quad (3.14)$$

where the covariant derivative for Σ is defined by

$$D_\mu \Sigma = \partial_\mu \Sigma - i\mu_q \delta_{\mu 0} (J\Sigma + \Sigma J^T) \quad \text{with} \quad J = \begin{pmatrix} \mathbf{1} & 0 \\ 0 & -\mathbf{1} \end{pmatrix}. \quad (3.15)$$

Here, the quark chemical potential μ_q is incorporated in the covariant derivative through gauging the $U(1)_B$ baryon-number symmetry. Besides, V represents potential terms describing interactions among the hadrons, which is separated into three parts as

$$V = V_0 + V_{\text{sp}} + V_{\text{anom}}. \quad (3.16)$$

V_0 represents an invariant part under the Pauli-Gursey $SU(4)$ symmetry. When we include contributions up to the fourth order of Σ as widely done in the linear sigma model for three-color QCD, it takes the form of

$$V_0 = m_0^2 \text{tr}[\Sigma^\dagger \Sigma] + \lambda_1 (\text{tr}[\Sigma^\dagger \Sigma])^2 + \lambda_2 \text{tr}[(\Sigma^\dagger \Sigma)^2], \quad (3.17)$$

where m_0^2 is a mass parameter, and λ_1 and λ_2 are coupling constants controlling the strength of four point interactions. The second piece of Eq. (3.16), V_{sp} , is the spurion term corresponding to $\mathcal{L}_{\text{QC}_2\text{D}}^{(\text{sp})}$ in Eq. (3.8), which is given by

$$V_{\text{sp}} = -\bar{c} \text{tr}[\zeta_{\text{sp}}^\dagger \Sigma + \Sigma^\dagger \zeta_{\text{sp}}], \quad (3.18)$$

where the parameter \bar{c} is real, and has the mass dimension two. Although the V_{sp} is invariant under the $SU(4)$ transformation thanks to Eq. (3.7), the spurion field χ_{sp} must be replaced by its VEV in Eq. (3.9) so as to incorporate the effect of the finite quark mass in a final step for evaluating physical observables.

The last piece in the potential (3.16), V_{anom} , includes $U(1)_A$ anomalous contributions which is responsible for the gluonic part in the non-conservation law of the axial current: the second term of the right-hand side (RHS) of Eq. (2.11). Within our present model, the $U(1)_A$ anomalous term is expressed by the Kobayashi-Maskawa-'t Hooft (KMT)-type interaction, [66–69]

$$V_{\text{anom}} = -c(\det \Sigma + \det \Sigma^\dagger). \quad (3.19)$$

As demonstrated below, this anomalous term generates a mass difference between the pion and η meson in the vacuum [65], and plays an important role in driving a finite topological

susceptibility. It should be noted that the KMT-type interaction is described by four-incoming and four-outgoing quarks owing to the quark bilinear field $\Sigma_{ij} \sim \bar{\Psi}_j^T \sigma^2 \tau_c^2 \Psi_i$ based on the Pauli-Gursey $SU(4)$ symmetry. Thus, in hadronic-level diagrams, V_{anom} represents four-point interactions.

4 Topological susceptibility at low energy

General expressions and characteristics of the topological susceptibility in QC_2D have been reviewed in Sec. 2, and the linear sigma model, which describes hadrons in the low-energy regime of QC_2D , has been invented in Sec. 3. In this section, we explain our strategy to evaluate the topological susceptibility within our linear sigma model through matching with the underlying QC_2D theory.

4.1 Matching between low-energy effective model and underlying QC_2D

In Sec. 3 we have constructed the linear sigma model in order to describe the hadrons as low-energy excitations of underlying QC_2D . On the basis of the concept of the low-energy effective theory, the linear sigma model is equivalent to QC_2D in the low-energy regime through the generating functional:

$$Z_{QC_2D} = Z_{\text{LSM}} = \int [d\Sigma] \exp \left(i \int d^4x \mathcal{L}_{\text{LSM}} \right). \quad (4.1)$$

In this subsection, we discuss the matching of the physical quantities between the linear sigma model and underlying QC_2D based on Eq. (4.1). Note that we neglect spin-1 hadronic excitations such as the ρ meson in the low-energy theory Z_{LSM} , even though the mass spectrums of spin-1 mesons coexist with that of spin-0 mesons in the low-energy regime [74]. This is because the topological susceptibility is evaluated by only the susceptibility functions χ_π and χ_η as in Eq. (2.14), which do not include spin-1 operators. The spin-1 hadronic excitations would hardly contribute to the following results.

In a similar way to Eq. (2.3), the effective action of the linear sigma model is given by

$$\Gamma_{\text{LSM}} = -i \ln Z_{\text{LSM}}. \quad (4.2)$$

From the equivalence in Eq. (4.1), we have the following matching condition in terms of Γ 's:

$$\Gamma_{QC_2D} = \Gamma_{\text{LSM}}, \quad (4.3)$$

Here, we emphasize that both the effective actions Γ_{QC_2D} and Γ_{LSM} depend on the spurion field ζ_{sp} commonly to maintain the systematics of $SU(4)$ symmetry. In general, ζ_{sp} takes the form of

$$\zeta_{\text{sp}} = (\zeta_S^a - i\zeta_P^a)X^a E + (\zeta_{B'}^i - i\zeta_B^i)X^i E, \quad (4.4)$$

where ζ_S^a (ζ_P^a) are scalar (pseudoscalar) source fields, and ζ_B^i ($\zeta_{B'}^i$) are source fields associated with the positive-parity (negative-parity) diquark baryons.

Taking functional derivatives with respect to the source fields in both sides of Eq. (4.3), the matching between the linear sigma model and underlying QC₂D can be done. For instance, functional derivatives with respect to the scalar source field ζ_S^0 yield^{#2}

$$\begin{aligned} \langle \bar{\psi}\psi \rangle &= -\sqrt{2} \frac{\delta\Gamma_{\text{QC}_2\text{D}}}{\delta\zeta_S^0(x)} \Big|_{\zeta_{\text{sp}}=\langle\zeta_{\text{sp}}\rangle} \\ &= -\sqrt{2} \frac{\delta\Gamma_{\text{LSM}}}{\delta\zeta_S^0(x)} \Big|_{\zeta_{\text{sp}}=\langle\zeta_{\text{sp}}\rangle} = -\sqrt{2}\bar{c}\langle\sigma\rangle . \end{aligned} \quad (4.5)$$

This implies that the chiral condensate $\langle\bar{\psi}\psi\rangle$ serving as an order parameter of the spontaneous breakdown of chiral symmetry is evaluated by a VEV of σ meson within the linear sigma model. Moreover, one can see that the chiral condensate is rewritten as

$$\langle \bar{\psi}\psi \rangle = \left\langle \left(-\frac{1}{2} \Psi^T \sigma^2 \tau_c^2 E \Psi + \text{h.c.} \right) \right\rangle . \quad (4.6)$$

This shows that the chiral condensate is invariant under a transformation with h which is an element of $Sp(4)$ belonging to a subgroup of $SU(4)$,

$$h^T E h = E . \quad (4.7)$$

Hence, the symmetry-breaking pattern caused by the chiral condensate is $SU(4) \rightarrow Sp(4)$.

Likewise, when we take functional derivatives of Eq. (4.3) with respect to ζ_B^5 , the following equivalence is obtained:

$$\begin{aligned} \left\langle \left(-\frac{i}{2} \psi^T C \gamma_5 \tau_c^2 \tau_f^2 \psi + \text{h.c.} \right) \right\rangle &= -\sqrt{2} \frac{\delta\Gamma_{\text{QC}_2\text{D}}}{\delta\zeta_B^5(x)} \Big|_{\zeta_{\text{sp}}=\langle\zeta_{\text{sp}}\rangle} \\ &= -\sqrt{2} \frac{\delta\Gamma_{\text{LSM}}}{\delta\zeta_B^5(x)} \Big|_{\zeta_{\text{sp}}=\langle\zeta_{\text{sp}}\rangle} = -\sqrt{2}\bar{c}\langle B^5 \rangle , \end{aligned} \quad (4.8)$$

with the charge-conjugation operator $C = i\gamma^2\gamma^0$. This equation indicates that the diquark condensate $\langle\psi^T C \gamma_5 \tau_c^2 \tau_f^2 \psi\rangle$, which plays a role of the order parameter for the emergence of the baryon superfluid phases, is mimicked by a VEV of the diquark baryon field B^5 in the linear sigma model. Since B^5 carries a finite quark number, the quark-number conservation no longer holds in the superfluid phase. It should be noted that the common coefficient \bar{c} in Eqs. (4.5) and (4.8) is the result of the Pauli-Gursey $SU(4)$ symmetry which combines mesons and diquark baryons into the single multiplet.

At zero temperature, low-energy effective theories such as the linear sigma model undergo the baryon superfluid phase transition at the half value of the vacuum pion mass: $\mu_q^{\text{cr}} = m_\pi^{\text{vac}}/2$ [51, 53, 65]. Below this critical chemical potential, only the hadronic phase, where no diquark condensates emerge, is realized, and all thermodynamic quantities do not change against increment of μ_q . This stable behavior is often referred to as the Silver-Braze

^{#2}The quark mass term in Eq. (2.1) is now replaced by the spurion term (3.8).

property, and lattice simulations also support it [49]. Above the critical chemical potential μ_q^{cr} , the baryon superfluid phase transition occurs and accordingly, the baryonic density also arises there. Meanwhile, in the baryon superfluid phase, the chiral condensate begins to decrease with increasing the baryonic density, resulting in the (partial) restoration of chiral symmetry [51, 53, 65].

In what follows, we use

$$\sigma_0 \equiv \langle \sigma \rangle, \quad \Delta \equiv \langle B^5 \rangle, \quad (4.9)$$

to refer to the VEVs, where the phase of $\langle B^5 \rangle$ has been chosen to make Δ real.

In Eqs. (4.5) and (4.8), we have demonstrated how the QCD observables for VEVs of single local operators are matched with physical quantities of the linear sigma model: the chiral condensate and diquark condensate. The matching can be also done for two-point correlation functions by taking second functional derivatives in Eq. (4.3) with respect to the source fields. In fact, by performing functional derivatives appropriately, one can find that the η -meson and pion susceptibility functions, χ_η and χ_π defined in Eqs. (2.10) and (2.13), are related to two-point functions of the η meson and pion in the linear sigma model, respectively, as

$$\begin{aligned} \chi_\eta &= -2i \int d^4x \frac{\delta^2 \Gamma_{\text{QC}_2\text{D}}}{\delta \zeta_P^0(x) \delta \zeta_P^0(0)} \Bigg|_{\zeta_{\text{sp}} = \langle \zeta_{\text{sp}} \rangle} \\ &= -2i \int d^4x \frac{\delta^2 \Gamma_{\text{LSM}}}{\delta \zeta_P^0(x) \delta \zeta_P^0(0)} \Bigg|_{\zeta_{\text{sp}} = \langle \zeta_{\text{sp}} \rangle} = 2\bar{c}^2 \int d^4x \langle 0 | T \eta(x) \eta(0) | 0 \rangle, \end{aligned} \quad (4.10)$$

and

$$\begin{aligned} \chi_\pi \delta^{ab} &= -2i \int d^4x \frac{\delta^2 \Gamma_{\text{QC}_2\text{D}}}{\delta \zeta_P^a(x) \delta \zeta_P^b(0)} \Bigg|_{\zeta_{\text{sp}} = \langle \zeta_{\text{sp}} \rangle} \\ &= -2i \int d^4x \frac{\delta^2 \Gamma_{\text{LSM}}}{\delta \zeta_P^a(x) \delta \zeta_P^b(0)} \Bigg|_{\zeta_{\text{sp}} = \langle \zeta_{\text{sp}} \rangle} = 2\bar{c}^2 \int d^4x \langle 0 | T \pi^a(x) \pi^b(0) | 0 \rangle \quad (\text{for } a, b = 1, 2, 3). \end{aligned} \quad (4.11)$$

Using these matching equations, we will present analytic expressions of the meson susceptibility functions within our linear sigma model.

4.2 Topological susceptibility across baryon superfluid phase transition

In this subsection, we proceed with analytic evaluation of the topological susceptibility from the linear sigma model.

In this work, we employ the mean-field approximation where loop corrections of hadronic fluctuations have not been taken into account. The effective potential of the linear sigma model at the tree level is evaluated as

$$V_{\text{mean}} = -2\mu_q^2 \Delta^2 + \frac{m_0^2}{2} (\sigma_0^2 + \Delta^2) + \frac{8\lambda_1 + 2\lambda_2 - c}{32} (\sigma_0^2 + \Delta^2)^2 - \sqrt{2} m_l \bar{c} \sigma_0. \quad (4.12)$$

In this potential the VEV of the spurion field (3.9) as well as the mean fields (4.9) are inserted. In Eq. (4.12) the quark chemical potential μ_q appears in a quadratic term of Δ with a negative sign, indicating that the larger value of μ_q yields nonzero Δ leading to the baryon superfluid phase as mentioned in Sec. 4.1. The vacuum configurations are determined by stationary conditions of V_{mean} with respect to σ_0 and Δ :

$$\frac{\partial V_{\text{mean}}}{\partial \sigma_0} = 0, \quad \frac{\partial V_{\text{mean}}}{\partial \Delta} = 0, \quad (4.13)$$

and hadrons appear as fluctuation modes upon the vacuum characterized by the conditions (4.13). In this description, hadron masses are evaluated by quadratic terms of the fluctuations in the Lagrangian (3.14) with σ_0 and Δ included. For instance, the pion mass reads

$$m_\pi^2 = m_0^2 + \frac{8\lambda_1 + 2\lambda_2 - c}{8}(\sigma_0^2 + \Delta^2) = \frac{\sqrt{2}m_l\bar{c}}{\sigma_0}. \quad (4.14)$$

We note that the second equality in Eq. (4.14) is obtained by considering the stationary condition of σ_0 in Eq. (4.13).

When we approximate the pion two-point function $\langle 0|T\pi^a(x)\pi^b(0)|0\rangle$ at the tree level in the linear sigma model, the pion susceptibility function in Eq. (4.11) is evaluated to be

$$\chi_\pi = -2i\bar{c}^2 \frac{1}{m_\pi^2}. \quad (4.15)$$

Similarly, we employ the tree-level approximation for the η -meson two-point function $\langle 0|T\eta(x)\eta(0)|0\rangle$. However, since the violation of $U(1)_B$ baryon-number symmetry in the baryon superfluid phase causes the mixing among η meson, the negative-parity diquark B' and antidiquark \bar{B}' (or equivalently η , B'_4 and B'_5), the two-point function of the η meson is not simply given by $-i/m_\eta^2$ where the η mass is read from η^2 term of the η fluctuation from the vacuum. By taking into account the mixing structure, the inverse propagator matrix for the $\eta - B'_4 - B'_5$ sector in the momentum space at the rest frame $\mathbf{p} = \mathbf{0}$ is obtained as

$$i\mathbf{D}^{-1} = i \begin{pmatrix} D_{\eta\eta} & D_{\eta B'_4} & D_{\eta B'_5} \\ D_{B'_4\eta} & D_{B'_4 B'_4} & D_{B'_4 B'_5} \\ D_{B'_5\eta} & D_{B'_5 B'_4} & D_{B'_5 B'_5} \end{pmatrix}^{-1} = \begin{pmatrix} p_0^2 - m_\eta^2 & 0 & -m_{B'_5\eta}^2 \\ 0 & p_0^2 - m_{B'_4}^2 & 4i\mu_q p_0 \\ -m_{B'_5\eta}^2 & -4i\mu_q p_0 & p_0^2 - m_{B'_5}^2 \end{pmatrix}, \quad (4.16)$$

where we have defined the two-point functions D_{XY} by $D_{XY} = \text{F.T.}\langle 0|TX(x)Y(0)|0\rangle$ with $X, Y = \eta, B'_4$ and B'_5 , and the mass parameters read

$$\begin{aligned} m_\eta^2 &= m_\pi^2 + \frac{\lambda_2}{2}\Delta^2 + \frac{c}{4}(2\sigma_0^2 + \Delta^2), \\ m_{B'_5}^2 &= m_\pi^2 - 4\mu_q^2 + \frac{\lambda_2}{2}\sigma_0^2 + \frac{c}{4}(\sigma_0^2 + 2\Delta^2), \\ m_{B'_5\eta}^2 &= \frac{2\lambda_2 - c}{4}\sigma_0\Delta. \end{aligned} \quad (4.17)$$

Thus, inverting the matrix (4.16), one can find that $D_{\eta\eta}$ which is of interest now takes the form of

$$D_{\eta\eta}(p_0) = \sum_{i=1,2,3} \frac{iZ_{\phi_i}}{p_0^2 - m_{\phi_i}^2}. \quad (4.18)$$

In this expression, m_{ϕ_1} , m_{ϕ_2} and m_{ϕ_3} represent mass eigenvalues of the $\eta - B'_4 - B'_5$ sector, where the subscripts ϕ_1 , ϕ_2 and ϕ_3 stand for the corresponding eigenstates with which the masses satisfy $m_{\phi_1} > m_{\phi_2} > m_{\phi_3}$. The renormalization constants Z_{ϕ_i} in Eq. (4.18) are evaluated by

$$\begin{aligned} Z_{\phi_1} &= \frac{\mathcal{N}_{\eta\eta}(m_{\phi_1})}{(m_{\phi_1}^2 - m_{\phi_2}^2)(m_{\phi_1}^2 - m_{\phi_3}^2)}, \\ Z_{\phi_2} &= \frac{\mathcal{N}_{\eta\eta}(m_{\phi_2})}{(m_{\phi_2}^2 - m_{\phi_1}^2)(m_{\phi_2}^2 - m_{\phi_3}^2)}, \\ Z_{\phi_3} &= \frac{\mathcal{N}_{\eta\eta}(m_{\phi_3})}{(m_{\phi_3}^2 - m_{\phi_1}^2)(m_{\phi_3}^2 - m_{\phi_2}^2)}, \end{aligned} \quad (4.19)$$

with

$$\mathcal{N}_{\eta\eta}(p_0) = p_0^4 - 16\mu_q^2 p_0^2 - (m_{B'_4}^2 + m_{B'_5}^2)p_0^2 + m_{B'_4}^2 m_{B'_5}^2. \quad (4.20)$$

We note that the constants satisfy a condition $Z_{\phi_1} + Z_{\phi_2} + Z_{\phi_3} = 1$ reflecting the fraction conservation. Therefore, Z_{ϕ_i} correspond to the proportion of the mass eigenstates ϕ_i in the two-point function $D_{\eta\eta}$ while the information on the respective pole positions is read from $1/(p_0^2 - m_{\phi_i}^2)$ in Eq. (4.18).^{#3}

By using the η -meson propagator based on the mass eigenstates ϕ_i in Eq. (4.18), the η -meson susceptibility function is evaluated as

$$\chi_\eta = 2\bar{c}^2 D_{\eta\eta}(0) = \sum_{i=1,2,3} \chi_{\phi_i}, \quad (4.22)$$

with

$$\chi_{\phi_i} \equiv -2i\bar{c}^2 \frac{Z_{\phi_i}}{m_{\phi_i}^2}. \quad (4.23)$$

Since the susceptibility is defined at the low-energy limit: $p_0 = 0$, the susceptibilities χ_{ϕ_i} in Eq. (4.23) are written by $Z_{\phi_i}^2/m_{\phi_i}^2$ with the constant $-2i\bar{c}^2$. Therefore, the strength of χ_η is controlled by the combination of the renormalization constants Z_{ϕ_i} and the mass eigenvalues m_{ϕ_i} .

5 Fate of topological susceptibility in dense QC₂D

With the help of the susceptibility functions χ_π and χ_η obtained in Eqs. (4.15) and (4.22), the topological susceptibility χ_{top} is evaluated within our linear sigma model from Eq. (2.14):

$$\chi_{\text{top}} = \frac{im_l^2}{4} \left(\chi_\pi - \sum_{i=1,2,3} \chi_{\phi_i} \right). \quad (5.1)$$

^{#3}In Eq. (4.18) we have expressed $D_{\eta\eta}(p_0)$ in terms of three contributions of ϕ_1 , ϕ_2 and ϕ_3 so as to see roles of the mass eigenstates clearly. In the low-energy limit $p_0 = 0$, $D_{\eta\eta}(0)$ is of course equivalent to the simple form of

$$D_{\eta\eta}(0) = -i \frac{m_{B'_5}^2}{m_\eta^2 m_{B'_5}^2 - m_{B'_5 \eta}^4}, \quad (4.21)$$

which can be straightforwardly derived by evaluating the inverse matrix of $\eta - B'_5$ sector of Eq (4.16).

In this section, based on it, we show the numerical results of χ_{top} at finite μ_q .

5.1 $U(1)_A$ anomaly contribution and μ_q dependence of topological susceptibility

As explained at the end of Sec. 2, the topological susceptibility is substantially controlled by the $U(1)_A$ axial anomaly, i.e., the mass difference between the η meson and pion in low-energy QC₂D. For this reason, we particularly investigate χ_{top} at finite μ_q with the two cases of $m_\eta^{\text{vac}}/m_\pi^{\text{vac}} = 1$ and $m_\eta^{\text{vac}}/m_\pi^{\text{vac}} = 1.5$. The former corresponds to vanishing anomaly effects for the hadron spectrum, while the latter implies the substantial anomaly effects.

Mass ratio	c	λ_1	λ_2	m_0^2	$m_l\bar{c}/2$
$m_\eta^{\text{vac}}/m_\pi^{\text{vac}} = 1$	0	0	65.6	$-(693 \text{ MeV})^2$	$(364 \text{ MeV})^3$
$m_\eta^{\text{vac}}/m_\pi^{\text{vac}} = 1.5$	21.8	0	54.7	$-(373 \text{ MeV})^2$	$(364 \text{ MeV})^3$

Table 1. Fixed parameters for $m_\eta^{\text{vac}}/m_\pi^{\text{vac}} = 1$ and $m_\eta^{\text{vac}}/m_\pi^{\text{vac}} = 1.5$.

When we fix the mass ratio $m_\eta^{\text{vac}}/m_\pi^{\text{vac}}$, there remain four parameters to be determined. As inputs, we employ $m_\pi^{\text{vac}} = 738 \text{ MeV}$ and $m_{B'(\bar{B}')}^{\text{vac}} = 1611 \text{ MeV}$ from the recent lattice data [74]. Besides, based on the previous work [65], $\sigma_0^{\text{vac}} = 250 \text{ MeV}$ is used as another input as a typical value. For the last constraint, we take $\lambda_1 = 0$ corresponding to the large N_c limit since λ_1 term includes a double trace in the flavor space. With those inputs, the model parameters are fixed as in Table 1. The table indicates that m_η^{vac} becomes larger than m_π^{vac} only when $c \neq 0$. In other words, the KMT-type interaction mimicking the $U(1)_A$ anomaly effects in the linear sigma model generates the mass difference between the η meson and pion, as expected from underlying QC₂D.

In order to demonstrate typical phase structures at zero temperature and finite chemical potential described by the present linear sigma model, we depict μ_q dependences of the chiral condensate σ_0 and diquark condensate Δ in the panel (a) of Fig. 1 for the two parameter sets of Table 1. This figure clearly shows that the baryon superfluid phase emerges from $\mu_q^{\text{cr}} = m_\pi^{\text{vac}}/2$, and accordingly chiral symmetry begins to be restored. The mean field σ_0 decreases in the superfluid phase independently of the strength of the $U(1)_A$ anomaly effects, whereas the anomaly accelerates the increment of Δ there. We note that the smooth reduction of σ_0 in the superfluid phase is analytically evaluated as

$$\sigma_0 = \frac{m_l\bar{c}}{2\sqrt{2}}\mu_q^{-2}, \quad (5.2)$$

from the stationary conditions in Eq. (4.13). We also note that in the case of the nonlinear representation of the Nambu-Goldstone (NG) bosons, the vacuum manifold of the $SU(4)$ symmetry breaking is constrained as “ $\sigma_0^2 + \Delta^2 = (\text{constant})$ ” at the tree level which was found in Refs. [50, 51]. However, this is not the case in the linear representation [65].

Incidentally, Fig. 1 also depicts the μ_q dependence of the baryon number density ($\rho = 4\Delta^2\mu_q$) normalized by $16f_\pi^2m_\pi^{\text{vac}}$ in panel (b). The baryon number density is generated after

reaching the baryon superfluid phase. Owing to the increment of Δ , the baryon number density is enhanced by the $U(1)_A$ anomalous contribution.

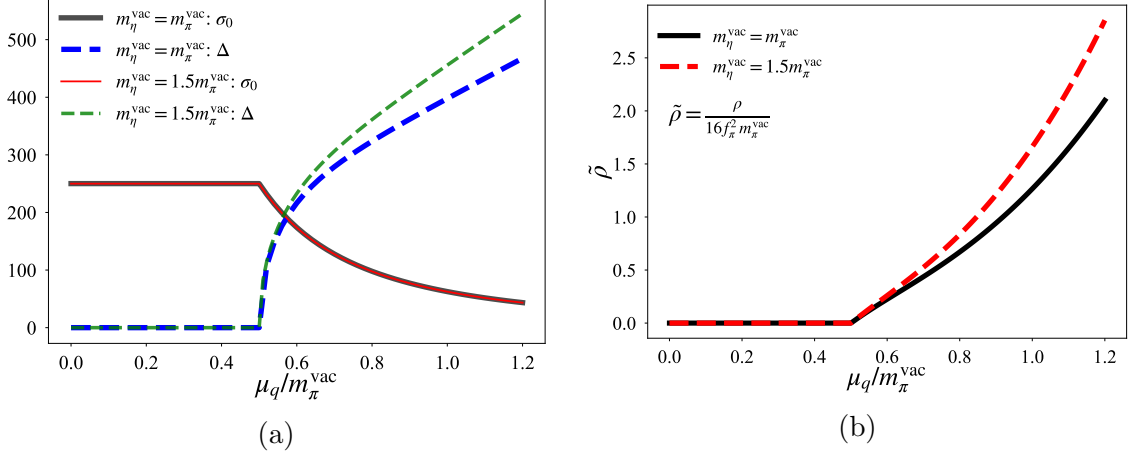


Figure 1. Chemical potential μ_q dependences of chiral condensate σ_0 and diquark condensate Δ (a) and that of the baryon density ρ normalized by $16f_\pi^2 m_\pi^{\text{vac}}$ (b).

For later convenience, here we comment on the masses m_{ϕ_i} and renormalization constants Z_{ϕ_i} across the phase transition. Displayed in Fig. 2 is μ_q dependences of the masses of η - B' - \bar{B}' sector for $m_\eta^{\text{vac}}/m_\pi^{\text{vac}} = 1$ (a) and $m_\eta^{\text{vac}}/m_\pi^{\text{vac}} = 1.5$ (b). In the baryon superfluid phase, m_{ϕ_1} , m_{ϕ_2} and m_{ϕ_3} correspond to the green curves from above: m_{ϕ_i} are ordered from the largest mass, $m_{\phi_1} > m_{\phi_2} > m_{\phi_3}$. Panel (b) in Fig. 2 indicates that the mass ordering of B' and η is interchanged below the critical chemical potential μ_q^{cr} for $m_\eta^{\text{vac}}/m_\pi^{\text{vac}} = 1.5$ whereas such a level crossing does not take place for $m_\eta^{\text{vac}}/m_\pi^{\text{vac}} = 1$. For this reason, the masses of ϕ_1 , ϕ_2 and ϕ_3 are connected to

$$\begin{aligned} (m_{\phi_1}, m_{\phi_2}, m_{\phi_3}) &\rightarrow (m_{\bar{B}'}, m_{B'}, m_\eta) && \text{for } m_\eta^{\text{vac}}/m_\pi^{\text{vac}} = 1, \\ (m_{\phi_1}, m_{\phi_2}, m_{\phi_3}) &\rightarrow (m_{\bar{B}'}, m_\eta, m_{B'}) && \text{for } m_\eta^{\text{vac}}/m_\pi^{\text{vac}} = 1.5, \end{aligned} \quad (5.3)$$

at μ_q^{cr} . These correspondences are also reflected in the renormalization constants Z_{ϕ_i} , as depicted in Fig. 3. Indeed, the figure indicates that in the hadronic phase the Z_{ϕ_i} are reduced to

$$\begin{aligned} (Z_{\phi_1}, Z_{\phi_2}, Z_{\phi_3}) &= (0, 0, 1) && \text{for } m_\eta^{\text{vac}}/m_\pi^{\text{vac}} = 1, \\ (Z_{\phi_1}, Z_{\phi_2}, Z_{\phi_3}) &= (0, 1, 0) && \text{for } m_\eta^{\text{vac}}/m_\pi^{\text{vac}} = 1.5. \end{aligned} \quad (5.4)$$

Thus, ϕ_3 (ϕ_2) state is connected to the η -meson state in this phase when $m_\eta^{\text{vac}}/m_\pi^{\text{vac}} = 1$ ($m_\eta^{\text{vac}}/m_\pi^{\text{vac}} = 1.5$). Meanwhile, in a limit of $\mu_q \rightarrow \infty$, both the parameter sets read $Z_{\phi_2} \rightarrow 1$ while $Z_{\phi_1}, Z_{\phi_3} \rightarrow 0$, reflecting a fact that the state of $\eta \sim \bar{\psi}i\gamma_5\psi$ is dominated by ϕ_2 solely at sufficiently large μ_q where σ_0 is negligible [65]. It should be noted that the ϕ_1 component in the η state is suppressed at any chemical potential.

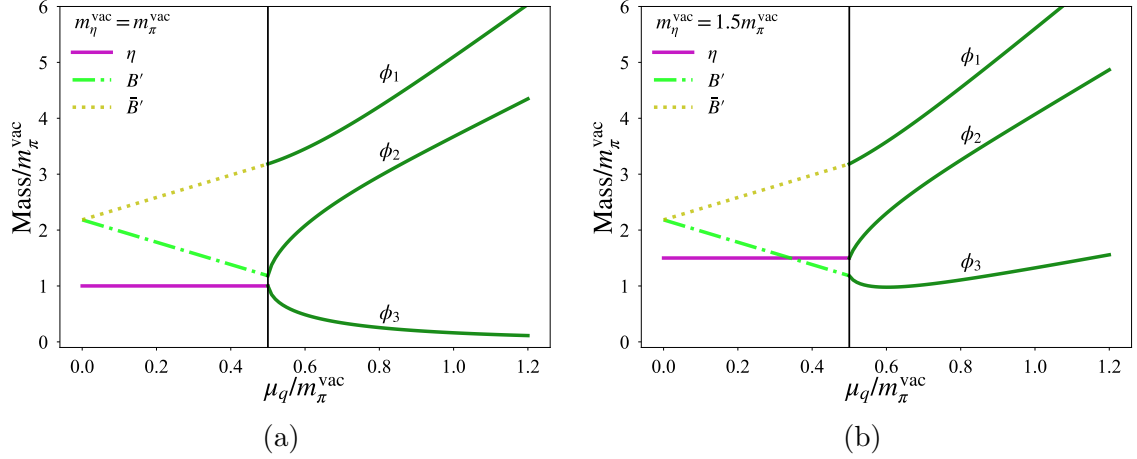


Figure 2. μ_q dependence of the masses of $\eta - B' - \bar{B}'$ sector for $m_\eta^{\text{vac}}/m_\pi^{\text{vac}} = 1$ (a) and $m_\eta^{\text{vac}}/m_\pi^{\text{vac}} = 1.5$ (b). In the baryon superfluid phase, m_{ϕ_1} , m_{ϕ_2} and m_{ϕ_3} correspond to the green curves from above. In this figure the hadron masses are scaled by m_π^{vac} .

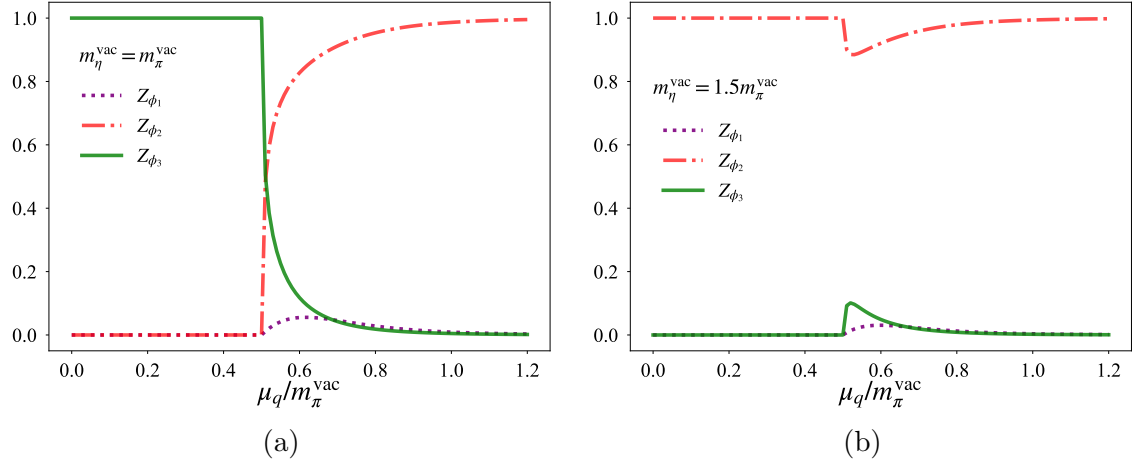


Figure 3. μ_q dependence of the renormalization constants Z_{ϕ_i} for $m_\eta^{\text{vac}}/m_\pi^{\text{vac}} = 1$ (a) and $m_\eta^{\text{vac}}/m_\pi^{\text{vac}} = 1.5$ (b).

Keeping the above properties in mind, we depict μ_q dependences of the topological susceptibility χ_{top} in Fig. 4. From panel (a) one can see the topological susceptibility is always zero in the absence of the $U(1)_A$ anomaly effects. In the hadronic phase, such a trend is easily understood by a fact that m_π^{vac} coincides with m_η^{vac} together with Eq. (2.14). The null topological susceptibility in the superfluid phase is rather surprising, but it is also understood as follows. Within our linear sigma model, the KMT-type interaction is introduced to mimic the gluonic anomalous part in the non-conservation law of the $U(1)_A$ axial current in Eq. (2.11). This structure is irrespective of changes of dynamical symmetry-breaking properties such as the emergence of the baryon superfluidity. Hence, even in the superfluid phase where the η meson mixes with B'_4 and B'_5 , the θ dependence in

the quark mass term in Eq. (2.8) would be rotated away under $U(1)_A$ transformation when the KMT-type interaction, i.e., the $U(1)_A$ anomaly effect, is turned off. For this reason, the topological susceptibility defined by a second derivative with respect to θ always vanishes as long as $c = 0$ is taken.

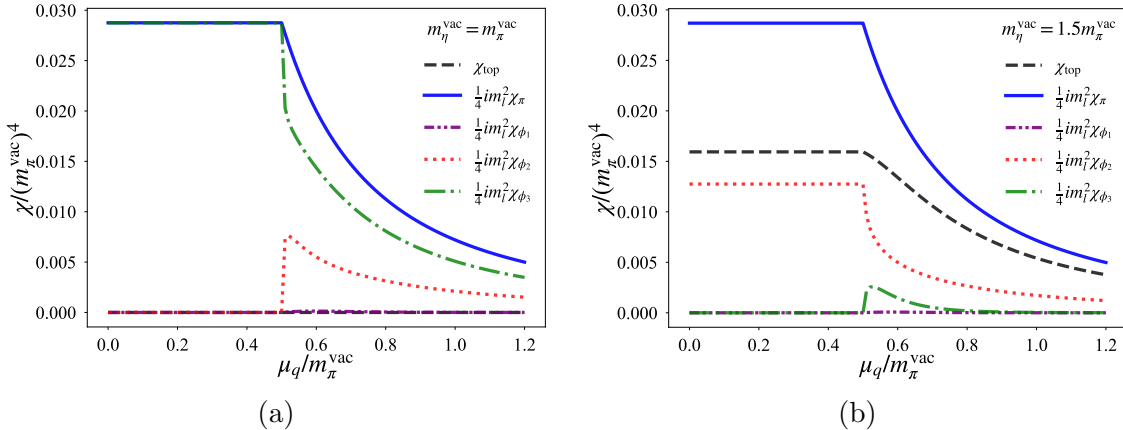


Figure 4. μ_q dependence of the topological susceptibility and the meson susceptibility functions for $m_\eta^{\text{vac}}/m_\pi^{\text{vac}} = 1$ (a) and $m_\eta^{\text{vac}}/m_\pi^{\text{vac}} = 1.5$ (b). In this figure, the susceptibilities are scaled by $(m_\pi^{\text{vac}})^4$.

Here, we comment on behaviors of the each contribution from χ_π and χ_{ϕ_i} in panel (a) of Fig. 4. First, since the pion mass in the baryon superfluid phase is expressed as

$$m_\pi^2 = 4\mu_q^2, \quad (5.5)$$

the pion susceptibility function χ_π decreases in this phase with a power of μ_q^{-2} . In contrast to the baryon superfluid phase, χ_π does not change in the hadronic phase. Next, the figure indicates that, in the hadronic phase, the η -meson susceptibility function is completely dominated by χ_{ϕ_3} , while χ_{ϕ_1} and χ_{ϕ_2} vanish there. Hence, χ_{ϕ_3} coincides with χ_π to yield $\chi_{\text{top}} = 0$. This behavior is understood by panel (a) of Fig. 3; the η state in the hadronic phase is connected to the ϕ_3 one solely. Moving on to the baryon superfluid phase, we find that χ_{ϕ_2} grows from zero and χ_{ϕ_3} becomes smaller than χ_π to compensate the growth. Although Fig. 3 exhibits the significant interchange of Z_{ϕ_2} with Z_{ϕ_3} above $\mu_q \sim 0.53m_\pi^{\text{vac}}$, χ_{ϕ_2} is smaller than χ_{ϕ_3} at any chemical potential due to the comparably strong suppression stemming from the $m_{\phi_2}^{-2}$ dependence in Eq. (4.23). Meanwhile, χ_{ϕ_1} is always negligible because of the large mass suppression of $1/m_{\phi_1}^2$ and the small value of Z_{ϕ_1} (see in Figs. 2 and Fig. 3).

The $U(1)_A$ anomaly effect represented by a nonzero c in our linear sigma model can be seen from panel (b) of Fig. 4, where $m_\eta^{\text{vac}}/m_\pi^{\text{vac}} = 1.5$ is taken. In the hadronic phase $m_\pi^{\text{vac}} < m_\eta^{\text{vac}}$ holds, and thus, χ_η becomes smaller than χ_π , resulting the nonzero topological susceptibility. In the baryon superfluid phase, χ_{top} decreases monotonically and approaches zero. The detailed analysis on this asymptotic behavior is provided in Sec. 5.2. Before taking a closer look at the smooth suppression of χ_{top} at larger μ_q , we explain behaviors of

the respective meson susceptibility functions in the presence of the KMT-type interaction. First, the μ_q dependence of χ_π remains the same as one without the $U(1)_A$ anomaly effects: the μ_q scaling of m_π in the superfluid phase, $m_\pi^2 = 4\mu_q^2$, holds even when the anomaly is included. Second, in the hadronic phase only χ_{ϕ_2} contributes to the topological susceptibility while χ_{ϕ_1} and χ_{ϕ_3} do not, as seen from panel (b) of Fig. 3. Third, in the superfluid phase, the finite χ_{ϕ_3} is induced above μ_q^{cr} owing to the bump structure of Z_{ϕ_3} shown in panel (b) of Fig. 3. But soon it begins to decrease and becomes negligible around $\mu_q \sim 0.8m_\pi^{\text{vac}}$ accompanied by the suppression of Z_{ϕ_3} . Meanwhile, the abrupt suppression of χ_{ϕ_2} occurs above μ_q^{cr} to compensate the enhancement of χ_{ϕ_3} , and at larger μ_q , χ_{ϕ_2} gradually approaches zero in accordance with the increment of m_{ϕ_2} . We note that χ_{ϕ_1} is almost zero at any chemical potential from the same reason explained for $m_\eta^{\text{vac}}/m_\pi^{\text{vac}} = 1$.

5.2 Asymptotic behavior of topological susceptibility in dense baryonic matter

Here, we focus on the cases for $m_\eta^{\text{vac}}/m_\pi^{\text{vac}} > 1$, in which the finite χ_{top} is provided, in order to delineate the asymptotic behavior of χ_{top} at larger μ_q .

The smooth reduction of χ_{top} at larger μ_q in panel (b) of Fig. 4 can be explained by the continuous reduction of $\langle \bar{\psi}\psi \rangle$, as inferred from Eq. (2.17).^{#4} In order to see this behavior, we rewrite the topological susceptibility to $\chi_{\text{top}} = (m_l \bar{c})^2 \delta_m / (8\mu_q^2)$ with the help of Eqs. (4.5) and (5.2). The dimensionless quantity δ_m is easily evaluated at sufficiently large μ_q with an assumption that χ_η is solely controlled by ϕ_2 state. Indeed, the asymptotic behavior of m_{ϕ_2} is known to be $m_{\phi_2}^2 \sim 12\mu_q^2$ [65], so that the quantity δ_m is approximated to be $\delta_m \sim 2/3$ with Eq. (5.5). Therefore, the asymptotic behavior of χ_{top} would be analytically fitted by

$$\frac{\chi_{\text{top}}}{(m_\pi^{\text{vac}})^4} \sim \frac{(f_\pi^{\text{vac}})^2}{12} \mu_q^{-2}, \quad (5.6)$$

where $(m_\pi^{\text{vac}})^2 = \sqrt{2}m_l \bar{c} / \sigma_0^{\text{vac}} = m_l \bar{c} / f_\pi^{\text{vac}}$ is used. The μ_q scaling of χ_{top} coincides with that of the chiral condensate in the superfluid phase [see Eq. (5.2)]. In Fig. 5, we plot the topological susceptibility in the baryon superfluid phase with several values of $m_\eta^{\text{vac}}/m_\pi^{\text{vac}}$ with keeping input values: $m_\pi^{\text{vac}} = 738\text{MeV}$, $m_{B(\bar{B})}^{\text{vac}} = 1611\text{MeV}$ and $\sigma_0^{\text{vac}} = 250\text{MeV}$. The figure shows that the asymptotic behavior of χ_{top} is fitted by the analytic expression in Eq. (5.6) well, regardless of the value of $m_\eta^{\text{vac}}/m_\pi^{\text{vac}}$.

^{#4}A similar smooth decrease of χ_{top} associated with the continuous chiral phase transition was observed in hot three-color QCD matter based on chiral model analyses [7, 8, 21], and lattice simulations at physical quark masses support such a behavior [10–12].

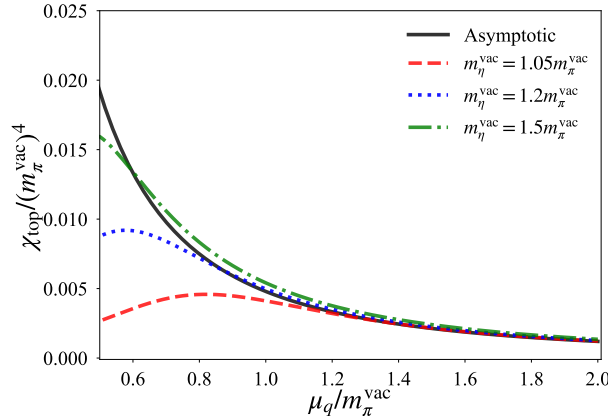


Figure 5. Topological susceptibility in the baryon superfluid phase with several values of $m_\eta^{\text{vac}}/m_\pi^{\text{vac}}$.

The lattice simulation performed in Ref. [41] at $T = 0.45T_c$ indicates that the topological susceptibility of QC₂D in the hadronic phase has a finite value with the error bars and is not influenced by the μ_q effect. ^{#5} Moreover, the lattice result shows that such an approximately μ_q -independent behavior is further extended to the baryon superfluid phase, which obviously contradicts our model estimations. One possible scenario explaining this discrepancy is discussed in Sec. 6. In contrast to Ref. [41], the other lattice result reported in Ref. [45] would suggest that the topological susceptibility in the baryon superfluid phase is suppressed, as estimated by our present study.

6 Contamination by diquark source field

In the evaluations in Sec. 5, we have included only the VEV of a scalar source field from the spurion field ζ_{sp} which turns into the current quark mass as shown in Eq. (3.9). On the other hand, in lattice simulations diquark source effects incorporated from a VEV of ζ_B^5 in Eq. (4.4) would remain additionally, particularly in the baryon superfluid phase. Then, in this section we discuss the diquark source effects to the topological susceptibility at finite μ_q within our linear sigma model.

6.1 Diquark source effect on topological susceptibility

To analytically find out contributions of the diquark source field j to the topological susceptibility, we first incorporate j in underlying QC₂D by adding the VEV of $\langle \zeta_B^5 \rangle = \sqrt{2}j$ from the spurion field (4.4). Now the VEV of ζ_{sp} reads

$$\langle \zeta_{\text{sp}} \rangle = \frac{m_l}{2} E - i\sqrt{2}j X^5 E. \quad (6.1)$$

^{#5}Here, T_c denotes the pseudocritical temperature for the chiral phase transition at vanishing μ_q , which are fixed to be $T_c = 200$ MeV [44].

With this VEV, a diquark operator tagged with the diquark source j shows up as a new ingredient in the quark mass term:

$$\mathcal{L}_{\text{QC}_2\text{D}}^{(\text{mass})} = -m_l \bar{\psi} \psi - j \left(-\frac{i}{2} \psi^T C \gamma_5 \tau_c^2 \tau_f^2 \psi + \text{h.c.} \right). \quad (6.2)$$

This mass term implies that the extra term characterized by j explicitly breaks the $U(1)_A$ symmetry as well as the $U(1)_B$ baryon-number symmetry. In fact, under the $U(1)_A$ axial transformation with an angle satisfying $\alpha_A = 2\theta$, the generating functional of QC₂D with the modified mass term (6.2) is rotated to

$$Z_{\text{QC}_2\text{D}} = \int [d\bar{\psi} d\psi] [dA] \exp \left[i \int d^4x \left(\bar{\psi} i \gamma^\mu D_\mu \psi - m_l \bar{\psi} \exp(i\theta/2 \gamma_5) \psi - j \left(-\frac{i}{2} \psi^T C \gamma_5 \tau_c^2 \tau_f^2 e^{i\theta/2 \gamma_5} \psi + \text{h.c.} \right) - \frac{1}{4} G_{\mu\nu}^a G^{\mu\nu, a} \right) \right], \quad (6.3)$$

and hence, from Eq. (2.4) via Eq. (2.3) the net topological susceptibility $\chi_{\text{top}}^{\text{w/j}}$ is evaluated to be

$$\chi_{\text{top}}^{\text{w/j}} = \chi_{\text{top}}^{(\text{M})} + \delta\chi_{\text{top}}. \quad (6.4)$$

In this expression, $\chi_{\text{top}}^{(\text{M})}$ is identical to χ_{top} given by Eq. (2.14), but here the superscript “(M)” has been attached in order to emphasize that only contributions from the meson susceptibility functions are included:

$$\chi_{\text{top}}^{(\text{M})} = \frac{i}{4} m_l^2 (\chi_\pi - \chi_\eta). \quad (6.5)$$

$\delta\chi_{\text{top}}$ denotes additional contributions from j which is of the form

$$\delta\chi_{\text{top}} = -\frac{1}{4} \left[j \left(-\frac{i}{2} \langle \psi^T C \gamma_5 \tau_c^2 \tau_f^2 \psi \rangle + \text{h.c.} \right) + ij^2 \chi_{B_5'} - 2ijm_l \chi_{B_5' \eta} \right], \quad (6.6)$$

where $\chi_{B_5'}$ and $\chi_{B_5' \eta}$ represent a susceptibility function for the B_5' channel and a mixed one between the η and B_5' channels, respectively. Those contributions are defined by

$$\begin{aligned} \chi_{B_5'} &= \int d^4x \langle 0 | T \left(-\frac{1}{2} \psi^T C \tau_c^2 \tau_f^2 \psi + \text{h.c.} \right) (x) \left(-\frac{1}{2} \psi^T C \tau_c^2 \tau_f^2 \psi + \text{h.c.} \right) (0) | 0 \rangle, \\ \chi_{B_5' \eta} &= \int d^4x \langle 0 | T \left(\bar{\psi} i \gamma_5 \psi \right) (x) \left(-\frac{1}{2} \psi^T C \tau_c^2 \tau_f^2 \psi + \text{h.c.} \right) (0) | 0 \rangle. \end{aligned} \quad (6.7)$$

The additional contributions (6.6) can be further reduced. That is, using an identity

$$-\frac{i}{2} \langle \psi^T C \gamma_5 \tau_c^2 \tau_f^2 \psi \rangle + \text{h.c.} = -ij \chi_{B_4}, \quad (6.8)$$

with

$$\chi_{B_4} = \int d^4x \langle 0 | T \left(\frac{1}{2} \psi^T C \gamma_5 \tau_c^2 \tau_f^2 \psi + \text{h.c.} \right) (x) \left(\frac{1}{2} \psi^T C \gamma_5 \tau_c^2 \tau_f^2 \psi + \text{h.c.} \right) (0) | 0 \rangle, \quad (6.9)$$

which is derived in Appendix B, the corrections $\delta\chi_{\text{top}}$ in Eq. (6.6) are rewritten in terms of the hadron susceptibility functions as

$$\delta\chi_{\text{top}} = \chi_{\text{top}}^{(\text{mix})} + \chi_{\text{top}}^{(\text{B})}, \quad (6.10)$$

where^{#6}

$$\chi_{\text{top}}^{(\text{mix})} = \frac{i}{2} m_l j \chi_{B_5' \eta}, \quad \chi_{\text{top}}^{(\text{B})} = \frac{i}{4} j^2 (\chi_{B_4} - \chi_{B_5'}). \quad (6.12)$$

It is interesting to note that the baryonic contribution $\chi_{\text{top}}^{(\text{B})}$ is proportional to the difference of χ_{B_4} and $\chi_{B_5'}$, which takes a partner structure similarly to $\chi_{\text{top}}^{(\text{M})}$ argued in Sec. 2; the baryon susceptibility functions χ_{B_4} and $\chi_{B_5'}$ are also transformed to each other under the $U(1)_B$ and $U(1)_A$ transformations. In the baryon sector, the partner structure reads

$$\begin{array}{ccc} \chi_{B_4} & \xleftrightarrow{U(1)_B} & \chi_{B_5} \\ U(1)_A \updownarrow & & \updownarrow U(1)_A \\ \chi_{B_4'} & \xleftrightarrow{U(1)_B} & \chi_{B_5'} \end{array}$$

as explicitly derived in Appendix A.

The susceptibility functions χ_{B_4} , $\chi_{B_5'}$ and $\chi_{B_5' \eta}$ in Eq. (6.10) are evaluated within our linear sigma model by tracing a similar procedure in obtaining χ_η and χ_π in Sec. 4.2. The B_4 mode does not mix with other hadrons in the low-energy limit, so χ_{B_4} is simply expressed by

$$\chi_{B_4} = -2i\bar{c}^2 \frac{1}{m_{B_4}^2}, \quad (6.13)$$

where $m_{B_4}^2 = m_\pi^2 - 4\mu_q^2$ [65]. Meanwhile, $\chi_{B_5'}$ and $\chi_{B_5' \eta}$ are evaluated as

$$\chi_{B_5'} = D_{B_5' B_5'}(0), \quad \chi_{B_5' \eta} = D_{B_5' \eta}(0), \quad (6.14)$$

by inverting the matrix (4.16), which may be expressed in terms of three contributions of ϕ_1 , ϕ_2 and ϕ_3 as done for $D_{\eta\eta}(0)$ in Eq. (4.18). Based on these expressions, we numerically investigate μ_q dependences of $\chi_{\text{top}}^{w/j}$ for several j in the next subsection.

^{#6}Utilizing the matching condition (4.8) and the stationary condition for Δ in the presence of j , one can show that the GOR-like relation with respect to the breakdown of $U(1)_B$ baryon-number symmetry reads $f_B^2 m_{B_4}^2 = -j \langle \psi\psi \rangle / 2$, with $f_B = \Delta / \sqrt{2}$ being the corresponding decay constant and $m_{B_4}^2 = m_\pi^2 - 4\mu_q^2$. Here, $\langle \psi\psi \rangle$ is identical to the LHS of Eq. (4.8). From this relation, $\chi_{\text{top}}^{(\text{B})}$ can be rewritten into

$$\chi_{\text{top}}^{(\text{B})} = \frac{f_B^2 m_{B_4}^2}{2} \delta_m^{(\text{B})}, \quad (6.11)$$

with $\delta_m^{(\text{B})} = 1 - \chi_{B_5'} / \chi_{B_4}$, analogous to the expression for the meson sector in Eq. (2.19).

It should be noted that the non-conservation law of the $U(1)_A$ current in Eq. (2.11) is now modified as

$$\partial_\mu j_A^\mu = 2m_l \bar{\psi} i \gamma_5 \psi + (j \psi^T C \tau_c^2 \tau_f^2 \psi + \text{h.c.}) + \frac{g^2}{16\pi^2} \epsilon^{\mu\nu\rho\sigma} G_{\mu\nu}^a G_{\rho\sigma}^a, \quad (6.15)$$

where corrections of the diquark operator $\psi^T C \tau_c^2 \tau_f^2 \psi$ accompanied by the diquark source j are present.

6.2 Diquark source effect on μ_q dependence of topological susceptibility

In the presence of the diquark source j , $U(1)_B$ baryon-number symmetry is explicitly broken even in the vacuum as understood from the modified quark mass term in Eq. (6.2). In other words, Δ would be always nonzero in our linear sigma model, so that the phase structures are expected to be modified from the ones for $j = 0$. Then, before showing numerical results of the topological susceptibility (6.4), first we explore μ_q dependences of σ_0 and Δ corresponding to the chiral condensate and the diquark condensate, to clarify the phase structures in the presence of j .

In Fig. 6, we show the μ_q dependence of the mean fields for $j/m_l = 0.05$ and 0.18 with $m_\eta^{\text{vac}}/m_\pi^{\text{vac}} = 1$ (a) and $m_\eta^{\text{vac}}/m_\pi^{\text{vac}} = 1.5$ (b). The figure indicates that the definite phase transition with respect to the baryon superfluidity disappears and the value of Δ continuously increases for $j \neq 0$, whereas the second-order phase transition has certainly occurred for $j = 0$ as seen from Fig. 1. Accompanied by such a continuous change of Δ , σ_0 also shows a similar smooth change. Besides, Fig. 6 indicates that σ_0 at $\mu_q \sim 0$ is not significantly affected by the size of j while Δ is significantly affected. This is because the diquark source field j induces an additional tadpole term of Δ in the effective potential in Eq. (4.12) which only contributes to the stationary condition of Δ directly. Meanwhile, in the high-density region, j contributions become negligible due to large μ_q , so that the behavior of σ_0 (Δ) including the j effect merges into the one for $j = 0$ there.

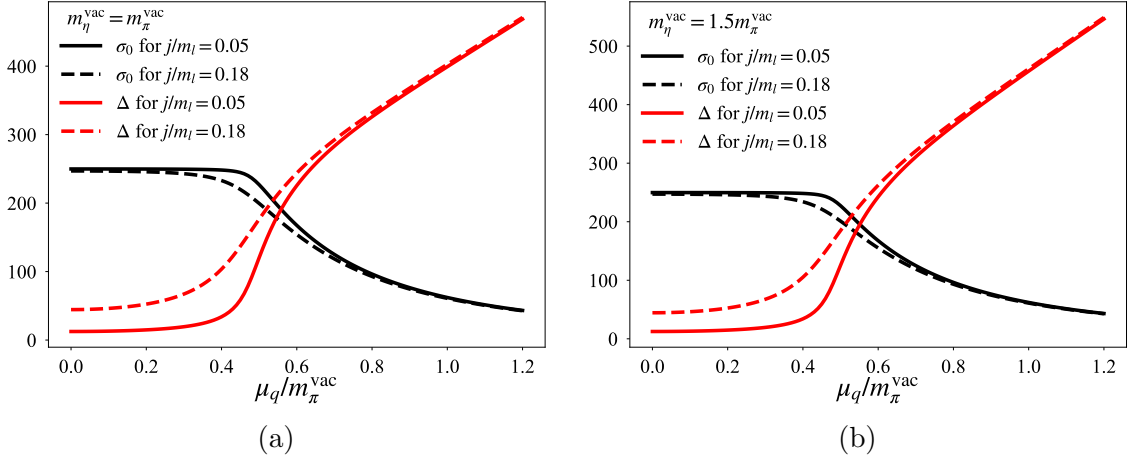


Figure 6. μ_q dependences of σ_0 and Δ for $j/m_l = 0.05$ and 0.18 with $m_\eta^{\text{vac}}/m_\pi^{\text{vac}} = 1$ (a) and $m_\eta^{\text{vac}}/m_\pi^{\text{vac}} = 1.5$ (b).

Next, we show the diquark source effects on the topological susceptibility in Figs. 7 and 8. Figure 7 exhibits the μ_q dependence of the topological susceptibility including diquark source effects in the absence of the KMT-type interaction: $m_\eta^{\text{vac}}/m_\pi^{\text{vac}} = 1$. As depicted in panel (a), the net topological susceptibility $\chi_{\text{top}}^{\text{w/j}}$ is null at any μ_q regardless of the value of j . This is because the gluonic $U(1)_A$ anomaly is mimicked by only the KMT-type interaction in the linear sigma model even with the diquark source field j . We also analyze each component of the net topological susceptibility, $\chi_{\text{top}}^{(\text{M})}$, $\chi_{\text{top}}^{(\text{mix})}$ and $\chi_{\text{top}}^{(\text{B})}$ defined in Eqs. (6.5) and (6.12) for $j/m_l = 0.18$, in panel (b). This panel clearly shows that the susceptibilities satisfy the relation $\chi_{\text{top}}^{(\text{M})} = \chi_{\text{top}}^{(\text{B})} = -\frac{1}{2}\chi_{\text{top}}^{(\text{mix})}$ to result in the null $\chi_{\text{top}}^{\text{w/j}}$. This notable relation can be analytically derived from the anomalous WTI associated with the $U(1)_A$ transformation as shown in Appendix C.

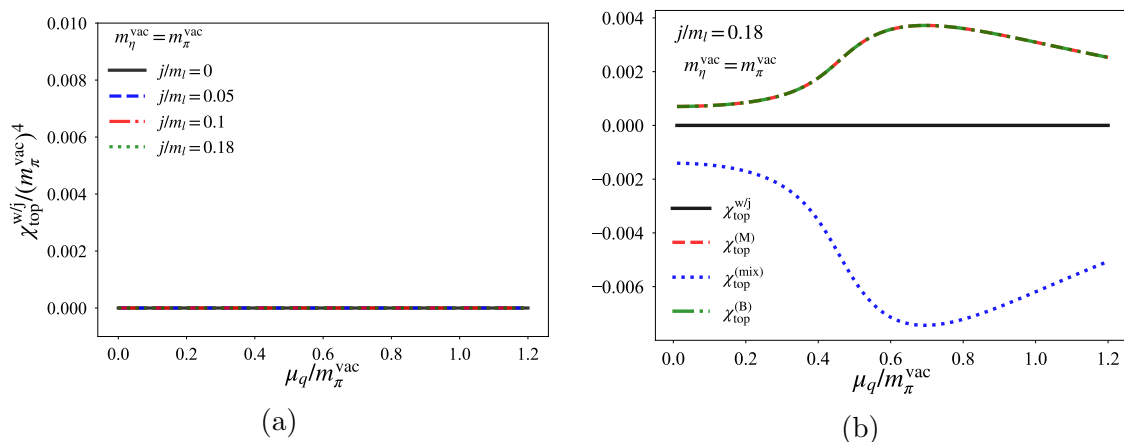


Figure 7. μ_q dependences of the topological susceptibility including the diquark source effects in the absence of the KMT-type interaction: $m_\eta^{\text{vac}}/m_\pi^{\text{vac}} = 1$.

By taking the KMT-type interaction into account, the net topological susceptibility $\chi_{\text{top}}^{\text{w/j}}$ becomes sensitive to the diquark source field especially above $\mu_q \approx m_\pi^{\text{vac}}/2$ as depicted in Fig. 8. Panel (a) shows that the decreasing trend of $\chi_{\text{top}}^{\text{w/j}}$ at higher μ_q is hindered as we take the larger value of j . Notably, when taking $j/m_l = 0.18$, the net topological susceptibility approximately holds the vacuum value at any μ_q . To grasp this behavior, we show separate contributions of $\chi_{\text{top}}^{(\text{M})}$, $\chi_{\text{top}}^{(\text{B})}$ and $\chi_{\text{top}}^{(\text{mix})}$ with $j/m_l = 0.18$ in panel (b) of Fig. 8. This figure indicates that $\chi_{\text{top}}^{(\text{M})}$ is not substantially influenced by the diquark source and its decreasing behavior is governed by the smooth chiral restoration as explained in Sec. 5.2 in detail. In contrast, $\chi_{\text{top}}^{(\text{B})}$ is enhanced above $\mu_q \approx m_\pi^{\text{vac}}/2$, which is understood by the increment of Δ . In fact, from the matching condition (4.8) and the stationary condition for Δ in the presence of j , one can easily show $\chi_{\text{top}}^{(\text{B})} = (j\bar{c})\Delta\delta_m^{(\text{B})}/(2\sqrt{2})$ with $\delta_m^{(\text{B})} = 1 - \chi_{B_5}'/\chi_{B_4}$. Here, similarly to the discussion for the meson sector in Sec. 5.2, $\delta_m^{(\text{B})}$ approaches a constant value asymptotically in the high-density region. Therefore, we can prove that the growth of $\chi_{\text{top}}^{(\text{B})}$ can be determined by Δ at larger μ_q . Hence, when the source contribution is sufficiently large, the net topological susceptibility can grow with

increasing μ_q . The last contribution, $\chi_{\text{top}}^{(\text{mix})}$, represents a mixing susceptibility between the mesonic and baryonic sectors, and this is suppressed compared to $\chi_{\text{top}}^{(M)}$ and $\chi_{\text{top}}^{(B)}$, as long as j is small, as shown in the figure. We note that, the mixing strength of B'_5 and η becomes weak for larger value of c as seen from $m_{B'_5\eta}^2$ in Eq. (4.17), and hence, the larger c we take, the smaller $\chi_{\text{top}}^{(\text{mix})}$ we obtain.

To summarize, from the demonstration in this subsection, we have revealed that the diquark source j contaminates the fate of the net topological susceptibility linked with the chiral restoration. Therefore, one can infer that the approximately μ_q -independent behavior of the topological susceptibility exhibited by the lattice data [41] would be understood by the finite diquark source effects. Note that although the approximately μ_q -independent behavior was found on the lattice at $T = 0.45T_c$, the temperature effects are expected to be insignificant. This is because the phase structure at $T = 0.45T_c$ does not significantly differ from one at $T = 0$.

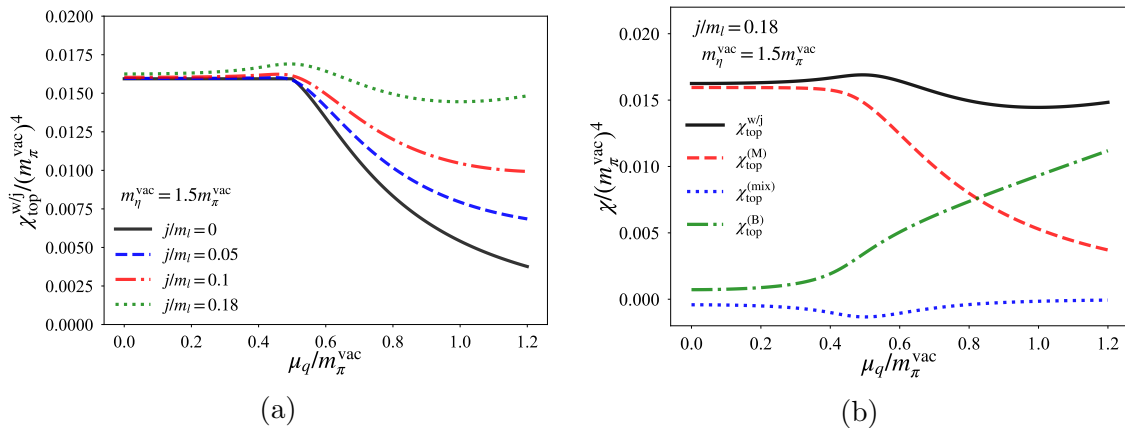


Figure 8. μ_q dependences of the topological susceptibility including the diquark source effects with the substantial anomaly effect of KMT-type interaction: $m_\eta^{\text{vac}}/m_\pi^{\text{vac}} = 1.5$.

7 Summary and discussion

In this paper, we have explored the topological susceptibility in QC_2D with two flavors at finite quark chemical potential μ_q , to clarify the $U(1)_A$ anomaly properties in cold and dense matter. With the help of the WTIs, we have found that the topological susceptibility is analytically expressed by a difference of the pion and η -meson susceptibility functions with the current quark mass. We have also argued that, in the low-energy regime, this expression is understood as a generalization of the one invented by Leutwyler and Smilga based on the ChPT in three-color QCD [72].

In order to investigate the topological susceptibility at finite μ_q , we have employed the linear sigma model in which the $U(1)_A$ anomaly effects are captured by the KMT-type determinant term, as a suitable low-energy effective theory of QC_2D [65]. This model successfully not only describes the emergence of the baryon superfluid phase but also reproduce the hadron mixings originated from the breakdown of $U(1)_B$ baryon-number

symmetry there, which is indeed suggested by the lattice data [74]. Based on a mean-field treatment, we have found that the topological susceptibility is always zero at any μ_q in both the hadronic and superfluid phases in the absence of the $U(1)_A$ anomaly effects, where the vacuum mass of pion coincides with one of η meson. When the $U(1)_A$ anomaly effect is switched on, the nonzero and constant topological susceptibility is induced in the hadronic phase. Moving on to the superfluid phase, we have found that it begins to smoothly decrease with increasing μ_q . We have analytically clarified that the latter smooth decrement is fitted by μ_q^{-2} at larger μ_q , reflecting the continuous restoration of chiral symmetry. This property is qualitatively the same as in hot three-color QCD matter [7, 8, 10–12, 21]. From those examinations, we can conclude that, in cold and dense QC₂D, roles of the topological susceptibility as an indicator for measuring the strength of $U(1)_A$ anomaly effects do not differ from those in hot three-color QCD, despite the complexity of phase structure due to the presence of the superfluidity.

In lattice simulations, effects from the diquark source would remain sizable. For this reason, we have further investigated the topological susceptibility in the presence of the diquark source. From this examination, we have revealed that the source effects enhance the topological susceptibility in accordance with the growth of the diquark condensate as μ_q increases, such that the reduction of the topological susceptibility found in the presence of the $U(1)_A$ anomaly effects can be hindered. Hence, when the source contribution is sufficiently large, the topological susceptibility can grow with increasing μ_q . On the other hand, when the $U(1)_A$ anomaly effects are absent, the topological susceptibility vanishes at any value of μ_q consistently regardless of the size of the diquark source.

In closing, we give a list of some comments on our findings and its implications.

- As argued in the later part of Sec. 2 in detail, the topological susceptibility in the vacuum is determined by only three basic observables: the pion decay constant, pion mass and η mass, in the low-energy regime of QC₂D. Thus, in order to pursue a consistent understanding of $U(1)_A$ anomaly effects in low-energy QC₂D, we expect precise determination of both the decay constant and the η mass as well as that of the topological susceptibility itself from lattice simulations. Those determinations would be regarded as a foundation toward more quantitative description of the topological susceptibility at finite μ_q .
- In the present analysis, we have used the linear sigma model based on a mean-field approach, and hence, all coupling constants in the model do not change at any μ_q . On the basis of the functional renormalization group (FRG) method in three-color QCD, it was suggested that the coupling strength of the KMT-type interaction can be enhanced in medium, leading to the effective enhancement of the $U(1)_A$ anomaly effects [75–78]. If this is the case, then the topological susceptibility can also be enhanced at finite μ_q . Hence, analyses from effective models beyond the mean-field level such as the FRG method, in which fluctuations of the hadrons are non-perturbatively incorporated, are worth studying.

- In our present study, we have focused on the topological susceptibility at finite μ_q but with zero temperature. Currently, the μ_q dependence on the topological susceptibility around the critical temperature has been also evaluated in the lattice QCD [41]. Thus, it would be worth investigating finite temperature effects to the topological susceptibility to fit the lattice data, to pursue more comprehensive description of the $U(1)_A$ anomaly effects on the phase diagram of QC₂D.
- In this study, we have clarified that the asymptotic behavior of the topological susceptibility at larger μ_q is mostly determined by the smooth reduction of the chiral condensate, despite the presence of the diquark condensate in dense QC₂D. This structure is essentially understood by a fact that the WTIs used to express the topological susceptibility in terms of the meson susceptibility functions are not altered by the diquark condensate, unless the diquark source contributions remain finite. In ordinary three-color QCD, on the other hand, the WTI associated with the pion would be modified in the color-flavor locking (CFL) phase, since the CFL configuration changes the chiral-symmetry breaking pattern due to correlations from $SU(3)_c$ color symmetry [79]. For this reason, it is not clear whether a similar asymptotic behavior is derived in cold and dense three-color QCD matter, and we leave this issue for a future study. Meanwhile, the two-flavor color superconductivity (2SC) is singlet under chiral symmetry, and hence, at intermediate density regime one can expect that a qualitatively similar behavior of the topological susceptibility follows even in the presence of the 2SC phase.

Acknowledgment

This work of M.K. is supported in part by the National Natural Science Foundation of China (NSFC) Grant Nos: 12235016, and the Strategic Priority Research Program of Chinese Academy of Sciences under Grant No XDB34030000. D.S. is supported by the RIKEN special postdoctoral researcher program. The authors thank K. Iida and E. Itou for fruitful discussion and useful information on their lattice results of the topological susceptibility.

A Partner structures of the susceptibility functions

In this appendix, we derive partner structures of the meson and diquark-baryon susceptibility functions with respect to appropriate transformations.

Here, we define the following composite operators

$$\begin{aligned}
\mathcal{O}_\sigma &\equiv \bar{\psi}\psi, \quad \mathcal{O}_{a_0}^a \equiv \bar{\psi}\tau_f^a\psi, \quad \mathcal{O}_\eta \equiv \bar{\psi}i\gamma_5\psi, \quad \mathcal{O}_\pi^a \equiv \bar{\psi}i\gamma_5\tau_f^a\psi, \\
\mathcal{O}_{B_4} &\equiv \frac{1}{2}\psi^T C\gamma_5\tau_c^2\tau_f^2\psi + \text{h.c.}, \quad \mathcal{O}_{B_5} \equiv -\frac{i}{2}\psi^T C\gamma_5\tau_c^2\tau_f^2\psi + \text{h.c.}, \\
\mathcal{O}_{B'_4} &= -\frac{i}{2}\psi^T C\tau_c^2\tau_f^2\psi - \frac{i}{2}\psi^\dagger C\tau_c^2\tau_f^2\psi^*, \quad \mathcal{O}_{B'_5} = -\frac{1}{2}\psi^T C\tau_c^2\tau_f^2\psi + \frac{1}{2}\psi^\dagger C\tau_c^2\tau_f^2\psi^*.
\end{aligned}
\tag{A.1}$$

The $U(1)_B$, $SU(2)_V$, $U(1)_A$ and $SU(2)_A$ rotations are generated by ($a = 1, 2, 3$)

$$\psi \xrightarrow{U(1)_B} e^{-i\epsilon_B} \psi, \quad \psi \xrightarrow{SU(2)_V} e^{-i\epsilon_V^a T_f^a} \psi, \quad \psi \xrightarrow{U(1)_A} e^{-i\epsilon_A \gamma_5} \psi, \quad \psi \xrightarrow{SU(2)_A} e^{-i\epsilon_A^a T_f^a} \psi, \quad (\text{A.2})$$

respectively. Then, the meson operators \mathcal{O}_σ , $\mathcal{O}_{a_0}^a$, \mathcal{O}_η and \mathcal{O}_π^a are invariant under the $U(1)_B$ and $SU(2)_V$ rotations, while under the infinitesimal $U(1)_A$ and $SU(2)_A$ ones they transform as

$$\begin{aligned} \mathcal{O}_\sigma &\xrightarrow{U(1)_A} \mathcal{O}_\sigma - 2\epsilon_A \mathcal{O}_\eta, & \mathcal{O}_{a_0}^a &\xrightarrow{U(1)_A} \mathcal{O}_{a_0}^a - 2\epsilon_A \mathcal{O}_\pi^a, \\ \mathcal{O}_\eta &\xrightarrow{U(1)_A} \mathcal{O}_\eta + 2\epsilon_A \mathcal{O}_\sigma, & \mathcal{O}_\pi^a &\xrightarrow{U(1)_A} \mathcal{O}_\pi^a + 2\epsilon_A \mathcal{O}_{a_0}^a, \end{aligned} \quad (\text{A.3})$$

and

$$\begin{aligned} \mathcal{O}_\sigma &\xrightarrow{SU(2)_A} \mathcal{O}_\sigma - \epsilon_A^a \mathcal{O}_\pi^a, & \mathcal{O}_{a_0}^a &\xrightarrow{SU(2)_A} \mathcal{O}_{a_0}^a - \epsilon_A^a \mathcal{O}_\eta, \\ \mathcal{O}_\eta &\xrightarrow{SU(2)_A} \mathcal{O}_\eta + \epsilon_A^a \mathcal{O}_{a_0}^a, & \mathcal{O}_\pi^a &\xrightarrow{SU(2)_A} \mathcal{O}_\pi^a + \epsilon_A^a \mathcal{O}_\sigma. \end{aligned} \quad (\text{A.4})$$

Hence, one can find the following partner structure

$$\begin{array}{ccc} & \xleftrightarrow{SU(2)} & \\ \chi_\pi & & \chi_\sigma \\ \uparrow & & \uparrow \\ U(1)_A & & U(1)_A \\ \downarrow & & \downarrow \\ \chi_{a_0} & \xleftrightarrow{SU(2)} & \chi_\eta \end{array}$$

where the susceptibility functions are defined by

$$\begin{aligned} \chi_\sigma &= \int d^4x \langle 0 | T \mathcal{O}_\sigma(x) \mathcal{O}_\sigma(0) | 0 \rangle, & \chi_{a_0} \delta^{ab} &= \int d^4x \langle 0 | T \mathcal{O}_{a_0}^a(x) \mathcal{O}_{a_0}^b(0) | 0 \rangle, \\ \chi_\eta &= \int d^4x \langle 0 | T \mathcal{O}_\eta(x) \mathcal{O}_\eta(0) | 0 \rangle, & \chi_\pi \delta^{ab} &= \int d^4x \langle 0 | T \mathcal{O}_\pi^a(x) \mathcal{O}_\pi^b(0) | 0 \rangle. \end{aligned} \quad (\text{A.5})$$

Meanwhile, the diquark-baryon operators \mathcal{O}_{B_4} , \mathcal{O}_{B_5} , $\mathcal{O}_{B'_4}$ and $\mathcal{O}_{B'_5}$ are invariant under the $SU(2)_V$ and $SU(2)_A$ rotations, while under the $U(1)_B$ and $U(1)_A$ ones they transform as

$$\begin{aligned} \mathcal{O}_{B_4} &\xrightarrow{U(1)_B} \mathcal{O}_{B_4} + 2\epsilon_B \mathcal{O}_{B_5}, & \mathcal{O}_{B_5} &\xrightarrow{U(1)_B} \mathcal{O}_{B_5} - 2\epsilon_B \mathcal{O}_{B_4}, \\ \mathcal{O}_{B'_4} &\xrightarrow{U(1)_B} \mathcal{O}_{B'_4} + 2\epsilon_B \mathcal{O}_{B'_5}, & \mathcal{O}_{B'_5} &\xrightarrow{U(1)_B} \mathcal{O}_{B'_5} - 2\epsilon_B \mathcal{O}_{B'_4}, \end{aligned} \quad (\text{A.6})$$

and

$$\begin{aligned} \mathcal{O}_{B_4} &\xrightarrow{U(1)_A} \mathcal{O}_{B_4} + 2\epsilon_A \mathcal{O}_{B'_4}, & \mathcal{O}_{B_5} &\xrightarrow{U(1)_A} \mathcal{O}_{B_5} + 2\epsilon_A \mathcal{O}_{B'_5}, \\ \mathcal{O}_{B'_4} &\xrightarrow{U(1)_A} \mathcal{O}_{B'_4} - 2\epsilon_A \mathcal{O}_{B_4}, & \mathcal{O}_{B'_5} &\xrightarrow{U(1)_A} \mathcal{O}_{B'_5} - 2\epsilon_A \mathcal{O}_{B_5}. \end{aligned} \quad (\text{A.7})$$

Hence, similarly to the meson sector, one can find the following partner structure

$$\begin{array}{ccc}
\chi_{B_4} & \xleftrightarrow{U(1)_B} & \chi_{B_5} \\
U(1)_A \updownarrow & & \updownarrow U(1)_A \\
\chi_{B'_4} & \xleftrightarrow{U(1)_B} & \chi_{B'_5}
\end{array}$$

where the susceptibility functions are defined by

$$\begin{aligned}
\chi_{B_4} &= \int d^4x \langle 0 | T \mathcal{O}_{B_4}(x) \mathcal{O}_{B_4}(0) | 0 \rangle, & \chi_{B_5} &= \int d^4x \langle 0 | T \mathcal{O}_{B_5}(x) \mathcal{O}_{B_5}(0) | 0 \rangle, \\
\chi_{B'_4} &= \int d^4x \langle 0 | T \mathcal{O}_{B'_4}(x) \mathcal{O}_{B'_4}(0) | 0 \rangle, & \chi_{B'_5} &= \int d^4x \langle 0 | T \mathcal{O}_{B'_5}(x) \mathcal{O}_{B'_5}(0) | 0 \rangle.
\end{aligned} \quad (\text{A.8})$$

The infinitesimal transformation laws obtained in this appendix play important roles in deriving the WTIs employed in the present paper.

B Derivation of WTIs (2.12) and (6.8)

In this appendix, we derive the WTIs in Eqs. (2.12) and (6.8) which allow us to rewrite the topological susceptibility in terms of only the hadron susceptibility functions.

Toward derivation of Eq. (2.12), we try to perform the $SU(2)_A$ rotation in the following path integral:

$$\mathcal{I}_\pi^a \equiv \int [d\bar{\psi}d\psi][dA] \mathcal{O}_\pi^a(y) e^{i \int d^4x \mathcal{L}_{\text{QC}_2\text{D}}}, \quad (\text{B.1})$$

where the QC₂D Lagrangian of interest here includes the diquark source term in addition to the mass term as

$$\mathcal{L}_{\text{QC}_2\text{D}} = \bar{\psi} i \not{D} \psi - m_l \mathcal{O}_\sigma - j \mathcal{O}_{B_5} - \frac{1}{4} G_{\mu\nu}^a G^{\mu\nu,a} + \theta \frac{g^2}{64\pi^2} \epsilon^{\mu\nu\rho\sigma} G_{\mu\nu}^a G_{\rho\sigma}^a. \quad (\text{B.2})$$

In this Lagrangian, the covariant derivative $D_\mu \psi = (\partial_\mu - i\mu_q \delta_{\mu 0} - ig A_\mu^a T_c^a) \psi$ describes contributions from the quark chemical potential μ_q and couplings with the gluons A_μ^a , and $G_{\mu\nu}^a = \partial_\mu A_\nu^a - \partial_\nu A_\mu^a + g \epsilon^{abc} A_\mu^b A_\nu^c$ is the gluon field strength. Under the infinitesimal local $SU(2)_A$ rotation, \mathcal{O}_π^a transforms as shown in Eq. (A.4), while the QC₂D Lagrangian exhibits the following transformation law:

$$\mathcal{L}_{\text{QC}_2\text{D}} \xrightarrow{SU(2)_A} \mathcal{L}_{\text{QC}_2\text{D}} + \frac{1}{2} (\partial_\mu \epsilon_A^a) j_A^{\mu,a} + m_l \epsilon_A^a \mathcal{O}_\pi^a, \quad (\text{B.3})$$

where $j_A^{\mu,a} \equiv \bar{\psi} \gamma^\mu \gamma_5 \tau_f^a \psi$ represents the axial current. Thus, under the same rotation, Eq. (B.1) transforms as

$$\begin{aligned}
\mathcal{I}_\pi^a \xrightarrow{SU(2)_A} & \mathcal{I}_\pi^a + \int [d\bar{\psi}d\psi][dA] \left\{ \epsilon_A^a(y) \mathcal{O}_\sigma(y) \right. \\
& \left. + i \int d^4x \epsilon_A^b(x) \left[-\frac{1}{2} \partial_\mu^x j_A^{\mu,b}(x) \mathcal{O}_\pi^a(y) + m_l \mathcal{O}_\pi^b(x) \mathcal{O}_\pi^a(y) \right] \right\} e^{i \int d^4x \mathcal{L}_{\text{QC}_2\text{D}}}, \quad (\text{B.4})
\end{aligned}$$

and imposing the invariance of \mathcal{I}_π^a under the $SU(2)_A$ transformation, one can obtain the following WTI

$$\langle \mathcal{O}_\sigma \rangle \delta^{ab} = i \int d^4x \left[\frac{1}{2} \partial_\mu^x \langle 0 | T j_A^{\mu,b}(x) \mathcal{O}_\pi^a(y) | 0 \rangle - m_l \langle 0 | T \mathcal{O}_\pi^b(x) \mathcal{O}_\pi^a(y) | 0 \rangle \right]. \quad (\text{B.5})$$

Here, since the QC₂D Lagrangian explicitly breaks $SU(2)_L \times SU(2)_R$ chiral symmetry, there is no room for massless modes coupled to the axial current $j_A^{\mu,b}$, so that the first term of the RHS in Eq. (B.5) trivially vanishes from the surface integral. Therefore, we arrive at

$$\langle \bar{\psi} \psi \rangle = -im_l \chi_\pi, \quad (\text{B.6})$$

with Eq. (A.5).

Similarly to the above derivation, the identity (6.8) is also derived by focusing on the $U(1)_B$ transformation of

$$\mathcal{I}_{B_4} \equiv \int [d\bar{\psi} d\psi] [dA] \mathcal{O}_{B_4}(y) e^{i \int d^4x \mathcal{L}_{\text{QC}_2\text{D}}}. \quad (\text{B.7})$$

In fact, under the infinitesimal local $U(1)_B$ rotation, \mathcal{O}_{B_4} transforms as in Eq. (A.6) and the QC₂D Lagrangian shows the following transformation law:

$$\mathcal{L}_{\text{QC}_2\text{D}} \xrightarrow{U(1)_B} \mathcal{L}_{\text{QC}_2\text{D}} + (\partial_\mu \epsilon_B) j_B^\mu + 2\epsilon_B j \mathcal{O}_{B_4}, \quad (\text{B.8})$$

where we have defined the vector current by $j_B^\mu \equiv \bar{\psi} \gamma^\mu \psi$. Thus, the $U(1)_B$ invariance of Eq. (B.7) yields

$$2\langle \mathcal{O}_{B_5} \rangle = i \int d^4x \left[\partial_\mu^x \langle 0 | T j_B^\mu(x) \mathcal{O}_{B_4}(y) | 0 \rangle - 2j \langle 0 | T \mathcal{O}_{B_4}(x) \mathcal{O}_{B_4}(y) | 0 \rangle \right]. \quad (\text{B.9})$$

Here, the first term of the RHS vanishes since no massless modes couple to the vector current j_B^μ owing to the presence of j term which violates $U(1)_B$ symmetry explicitly, and thus, one can obtain

$$-\frac{i}{2} \langle \psi^T C \gamma_5 \tau_c^2 \tau_f^2 \psi \rangle + \text{h.c.} = -ij \chi_{B_4} \quad (\text{B.10})$$

by defining

$$\chi_{B_4} = \int d^4x \langle 0 | T \mathcal{O}_{B_4}(x) \mathcal{O}_{B_4}(0) | 0 \rangle, \quad (\text{B.11})$$

with Eq. (A.8).

C Alternative expression of the topological susceptibility

In this appendix, we present an alternative expression of the topological susceptibility χ_{top} .

For this purpose, here, we consider the $U(1)_A$ transformations in the following two path integrals:

$$\begin{aligned}\mathcal{I}_\eta &\equiv \int [d\bar{\psi}d\psi][dA] \mathcal{O}_\eta(y) e^{i \int d^4x \mathcal{L}_{\text{QC}_2\text{D}}} , \\ \mathcal{I}_{B'_5} &\equiv \int [d\bar{\psi}d\psi][dA] \mathcal{O}_{B'_5}(y) e^{i \int d^4x \mathcal{L}_{\text{QC}_2\text{D}}} .\end{aligned}\tag{C.1}$$

Under the infinitesimal local $U(1)_A$ rotation, \mathcal{O}_η and $\mathcal{O}_{B'_5}$ transform as in Eqs. (A.3) and (A.7) while the QC_2D Lagrangian shows the following transformation law:

$$\mathcal{L}_{\text{QC}_2\text{D}} \xrightarrow{U(1)_A} \mathcal{L}_{\text{QC}_2\text{D}} - (\partial_\mu \epsilon_A) j_A^\mu + \epsilon_A (2m_l \mathcal{O}_\eta - 2j \mathcal{O}_{B'_5}) ,\tag{C.2}$$

with the flavor-singlet $U(1)_A$ axial current defined by $j_A^\mu \equiv \bar{\psi} \gamma^\mu \gamma_5 \psi$. Thus, tracing a similar procedure in deriving the WTIs (B.6) or (B.11), one can find

$$\begin{aligned}\langle \bar{\psi} \psi \rangle &= -i \left(m_l \chi_\eta - j \chi_{B'_5 \eta} + 2 \chi_{Q\eta} \right) , \\ -\frac{i}{2} \langle \psi^T C \gamma_5 \tau_c^2 \tau_f^2 \psi \rangle + \text{h.c.} &= i \left(m_l \chi_{B'_5 \eta} - j \chi_{B'_5} + 2 \chi_{QB'_5} \right) ,\end{aligned}\tag{C.3}$$

where we have defined mixed susceptibility functions by

$$\begin{aligned}\chi_{B'_5 \eta} &= \int d^4x \langle 0 | T \mathcal{O}_{B'_5}(x) \mathcal{O}_\eta(0) | 0 \rangle , \\ \chi_{Q\eta} &= \int d^4x \langle 0 | T Q(x) \mathcal{O}_\eta(0) | 0 \rangle , \\ \chi_{QB'_5} &= \int d^4x \langle 0 | T Q(x) \mathcal{O}_{B'_5}(0) | 0 \rangle ,\end{aligned}\tag{C.4}$$

with the gluonic topological operator $Q = (g^2/64\pi^2) \epsilon^{\mu\nu\rho\sigma} G_{\mu\nu}^a G_{\rho\sigma}^a$. It should be noted that the $U(1)_A$ anomaly contributions have been properly incorporated when performing the $U(1)_A$ axial transformation in \mathcal{I}_η and $\mathcal{I}_{B'_5}$ in Eq (C.1).

Here, using Eqs. (B.6) and (B.11), the anomalous WTIs in Eq. (C.3) are rewritten into

$$\chi_{\text{top}}^{(\text{M})} = -\frac{1}{2} \chi_{\text{top}}^{(\text{mix})} + \frac{i}{2} m_l \chi_{Q\eta} , \quad \chi_{\text{top}}^{(\text{B})} = -\frac{1}{2} \chi_{\text{top}}^{(\text{mix})} - \frac{i}{2} j \chi_{QB'_5} .\tag{C.5}$$

Therefore, when we suppose that the $U(1)_A$ anomaly effects can be neglected for some reason, the operator Q vanishes and

$$\chi_{\text{top}}^{(\text{M})} = \chi_{\text{top}}^{(\text{B})} = -\frac{1}{2} \chi_{\text{top}}^{(\text{mix})}\tag{C.6}$$

is satisfied. Indeed, this relation is consistent with the numerical results in Fig. 7 (a) where the $U(1)_A$ anomaly effects are absent.

References

- [1] Steven Weinberg. The $U(1)$ Problem. *Phys. Rev. D*, 11:3583–3593, 1975.

- [2] Michael Buballa. NJL model analysis of quark matter at large density. Phys. Rept., 407:205–376, 2005.
- [3] Gerard 't Hooft. How Instantons Solve the U(1) Problem. Phys. Rept., 142:357–387, 1986.
- [4] Tetsuo Hatsuda and Teiji Kunihiro. QCD phenomenology based on a chiral effective Lagrangian. Phys. Rept., 247:221–367, 1994.
- [5] A. Gómez Nicola and J. Ruiz de Elvira. Pseudoscalar susceptibilities and quark condensates: chiral restoration and lattice screening masses. JHEP, 03:186, 2016.
- [6] A. Gomez Nicola and J. Ruiz de Elvira. Patterns and partners for chiral symmetry restoration. Phys. Rev. D, 97(7):074016, 2018.
- [7] Mamiya Kawaguchi, Shinya Matsuzaki, and Akio Tomiya. Analysis of nonperturbative flavor violation at chiral crossover criticality in QCD. Phys. Rev. D, 103(5):054034, 2021.
- [8] Chuan-Xin Cui, Jin-Yang Li, Shinya Matsuzaki, Mamiya Kawaguchi, and Akio Tomiya. New interpretation of the chiral phase transition: Violation of the trilemma in QCD. Phys. Rev. D, 105(11):114031, 2022.
- [9] Chuan-Xin Cui, Mamiya Kawaguchi, Jin-Yang Li, Shinya Matsuzaki, and Akio Tomiya. New aspect of chiral and axial breaking in QCD. 5 2022.
- [10] Peter Petreczky, Hans-Peter Schadler, and Sayantan Sharma. The topological susceptibility in finite temperature QCD and axion cosmology. Phys. Lett. B, 762:498–505, 2016.
- [11] Sz. Borsanyi et al. Calculation of the axion mass based on high-temperature lattice quantum chromodynamics. Nature, 539(7627):69–71, 2016.
- [12] Claudio Bonati, Massimo D’Elia, Guido Martinelli, Francesco Negro, Francesco Sanfilippo, and Antonino Todaro. Topology in full QCD at high temperature: a multicanonical approach. JHEP, 11:170, 2018.
- [13] Thomas D. Cohen. The High temperature phase of QCD and U(1)-A symmetry. Phys. Rev. D, 54:R1867–R1870, 1996.
- [14] Sinya Aoki, Hidenori Fukaya, and Yusuke Taniguchi. Chiral symmetry restoration, eigenvalue density of Dirac operator and axial U(1) anomaly at finite temperature. Phys. Rev. D, 86:114512, 2012.
- [15] A. Tomiya, G. Cossu, S. Aoki, H. Fukaya, S. Hashimoto, T. Kaneko, and J. Noaki. Evidence of effective axial U(1) symmetry restoration at high temperature QCD. Phys. Rev. D, 96(3):034509, 2017. [Addendum: Phys.Rev.D 96, 079902 (2017)].
- [16] S. Aoki, Y. Aoki, G. Cossu, H. Fukaya, S. Hashimoto, T. Kaneko, C. Rohrhofer, and K. Suzuki. Study of the axial U(1) anomaly at high temperature with lattice chiral fermions. Phys. Rev. D, 103(7):074506, 2021.
- [17] Kei Suzuki, Sinya Aoki, Yasumichi Aoki, Guido Cossu, Hidenori Fukaya, Shoji Hashimoto, and Christian Rohrhofer. Axial U(1) symmetry and mesonic correlators at high temperature in $N_f = 2$ lattice QCD. PoS, LATTICE2019:178, 2020.
- [18] A. Bazavov et al. The chiral transition and $U(1)_A$ symmetry restoration from lattice QCD using Domain Wall Fermions. Phys. Rev. D, 86:094503, 2012.
- [19] Michael I. Buchoff et al. QCD chiral transition, U(1) $_A$ symmetry and the dirac spectrum using domain wall fermions. Phys. Rev. D, 89(5):054514, 2014.

- [20] Tanmoy Bhattacharya et al. QCD Phase Transition with Chiral Quarks and Physical Quark Masses. Phys. Rev. Lett., 113(8):082001, 2014.
- [21] Mamiya Kawaguchi, Shinya Matsuzaki, and Akio Tomiya. Nonperturbative flavor breaking in topological susceptibility at chiral crossover. Phys. Lett. B, 813:136044, 2021.
- [22] Gert Aarts. Introductory lectures on lattice QCD at nonzero baryon number. J. Phys. Conf. Ser., 706(2):022004, 2016.
- [23] Shin Muroya, Atsushi Nakamura, Chiho Nonaka, and Tetsuya Takaishi. Lattice QCD at finite density: An Introductory review. Prog. Theor. Phys., 110:615–668, 2003.
- [24] Simon Hands, John B. Kogut, Maria-Paola Lombardo, and Susan E. Morrison. Symmetries and spectrum of SU(2) lattice gauge theory at finite chemical potential. Nucl. Phys. B, 558:327–346, 1999.
- [25] J. B. Kogut, D. K. Sinclair, S. J. Hands, and S. E. Morrison. Two color QCD at nonzero quark number density. Phys. Rev. D, 64:094505, 2001.
- [26] Simon Hands, Istvan Montvay, Luigi Scorzato, and Jonivar Skullerud. Diquark condensation in dense adjoint matter. Eur. Phys. J. C, 22:451–461, 2001.
- [27] Shin Muroya, Atsushi Nakamura, and Chiho Nonaka. Behavior of hadrons at finite density: Lattice study of color SU(2) QCD. Phys. Lett. B, 551:305–310, 2003.
- [28] Shailesh Chandrasekharan and Fu-Jiun Jiang. Phase-diagram of two-color lattice QCD in the chiral limit. Phys. Rev. D, 74:014506, 2006.
- [29] Simon Hands, Seyong Kim, and Jon-Ivar Skullerud. Deconfinement in dense 2-color QCD. Eur. Phys. J. C, 48:193, 2006.
- [30] B. Alles, Massimo D’Elia, and M. P. Lombardo. Behaviour of the topological susceptibility in two colour QCD across the finite density transition. Nucl. Phys. B, 752:124–139, 2006.
- [31] Simon Hands, Peter Sitch, and Jon-Ivar Skullerud. Hadron Spectrum in a Two-Colour Baryon-Rich Medium. Phys. Lett. B, 662:405–412, 2008.
- [32] Simon Hands, Seyong Kim, and Jon-Ivar Skullerud. A Quarkyonic Phase in Dense Two Color Matter? Phys. Rev. D, 81:091502, 2010.
- [33] Simon Hands and Philip Kenny. Topological Fluctuations in Dense Matter with Two Colors. Phys. Lett. B, 701:373–377, 2011.
- [34] Seamus Cotter, Pietro Giudice, Simon Hands, and Jon-Ivar Skullerud. Towards the phase diagram of dense two-color matter. Phys. Rev. D, 87(3):034507, 2013.
- [35] Simon Hands, Seyong Kim, and Jon-Ivar Skullerud. Non-relativistic spectrum of two-color QCD at non-zero baryon density. Phys. Lett. B, 711:199–204, 2012.
- [36] Tamer Boz, Seamus Cotter, Leonard Fister, Dhagash Mehta, and Jon-Ivar Skullerud. Phase transitions and gluodynamics in 2-colour matter at high density. Eur. Phys. J. A, 49:87, 2013.
- [37] V. V. Braguta, E. M. Ilgenfritz, A. Yu. Kotov, A. V. Molochkov, and A. A. Nikolaev. Study of the phase diagram of dense two-color QCD within lattice simulation. Phys. Rev. D, 94(11):114510, 2016.
- [38] M. Pühr and P. V. Buividovich. Numerical Study of Nonperturbative Corrections to the Chiral Separation Effect in Quenched Finite-Density QCD. Phys. Rev. Lett., 118(19):192003,

2017.

- [39] Tamer Boz, Ouraman Hajizadeh, Axel Maas, and Jon-Ivar Skullerud. Finite-density gauge correlation functions in QC2D. *Phys. Rev. D*, 99(7):074514, 2019.
- [40] N. Yu. Astrakhantsev, V. G. Bornyakov, V. V. Braguta, E. M. Ilgenfritz, A. Yu. Kotov, A. A. Nikolaev, and A. Rothkopf. Lattice study of static quark-antiquark interactions in dense quark matter. *JHEP*, 05:171, 2019.
- [41] Kei Iida, Etsuko Itou, and Tong-Gyu Lee. Two-colour QCD phases and the topology at low temperature and high density. *JHEP*, 01:181, 2020.
- [42] Jonas Wilhelm, Lukas Holicki, Dominik Smith, Björn Wellegehausen, and Lorenz von Smekal. Continuum Goldstone spectrum of two-color QCD at finite density with staggered quarks. *Phys. Rev. D*, 100(11):114507, 2019.
- [43] P. V. Buividovich, D. Smith, and L. von Smekal. Numerical study of the chiral separation effect in two-color QCD at finite density. *Phys. Rev. D*, 104(1):014511, 2021.
- [44] Kei Iida, Etsuko Itou, and Tong-Gyu Lee. Relative scale setting for two-color QCD with $N_f=2$ Wilson fermions. *PTEP*, 2021(1):013B05, 2021.
- [45] N. Astrakhantsev, V. V. Braguta, E. M. Ilgenfritz, A. Yu. Kotov, and A. A. Nikolaev. Lattice study of thermodynamic properties of dense QC₂D. *Phys. Rev. D*, 102(7):074507, 2020.
- [46] V. G. Bornyakov, V. V. Braguta, A. A. Nikolaev, and R. N. Rogalyov. Effects of Dense Quark Matter on Gluon Propagators in Lattice QC₂D. *Phys. Rev. D*, 102:114511, 2020.
- [47] P. V. Buividovich, D. Smith, and L. von Smekal. Electric conductivity in finite-density $SU(2)$ lattice gauge theory with dynamical fermions. *Phys. Rev. D*, 102(9):094510, 2020.
- [48] P. V. Buividovich, D. Smith, and L. von Smekal. Static magnetic susceptibility in finite-density $SU(2)$ lattice gauge theory. *Eur. Phys. J. A*, 57(10):293, 2021.
- [49] Kei Iida and Etsuko Itou. Velocity of sound beyond the high-density relativistic limit from lattice simulation of dense two-color QCD. *PTEP*, 2022(11):111B01, 2022.
- [50] J. B. Kogut, Misha A. Stephanov, and D. Toublan. On two color QCD with baryon chemical potential. *Phys. Lett. B*, 464:183–191, 1999.
- [51] J. B. Kogut, Misha A. Stephanov, D. Toublan, J. J. M. Verbaarschot, and A. Zhitnitsky. QCD - like theories at finite baryon density. *Nucl. Phys. B*, 582:477–513, 2000.
- [52] J. T. Lenaghan, F. Sannino, and K. Splittorff. The Superfluid and conformal phase transitions of two color QCD. *Phys. Rev. D*, 65:054002, 2002.
- [53] Claudia Ratti and Wolfram Weise. Thermodynamics of two-colour QCD and the Nambu Jona-Lasinio model. *Phys. Rev. D*, 70:054013, 2004.
- [54] Gao-feng Sun, Lianyi He, and Pengfei Zhuang. BEC-BCS crossover in the Nambu-Jona-Lasinio model of QCD. *Phys. Rev. D*, 75:096004, 2007.
- [55] Tomas Brauner, Kenji Fukushima, and Yoshimasa Hidaka. Two-color quark matter: $U(1)(A)$ restoration, superfluidity, and quarkyonic phase. *Phys. Rev. D*, 80:074035, 2009. [Erratum: *Phys.Rev.D* 81, 119904 (2010)].
- [56] Takuya Kanazawa, Tilo Wettig, and Naoki Yamamoto. Chiral Lagrangian and spectral sum rules for dense two-color QCD. *JHEP*, 08:003, 2009.
- [57] Masayasu Harada, Chiho Nonaka, and Tetsuro Yamaoka. Masses of vector bosons in

- two-color dense QCD based on the hidden local symmetry. Phys. Rev. D, 81:096003, 2010.
- [58] Nils Strodthoff, Bernd-Jochen Schaefer, and Lorenz von Smekal. Quark-meson-diquark model for two-color QCD. Phys. Rev. D, 85:074007, 2012.
- [59] Daiki Suenaga and Toru Kojo. Gluon propagator in two-color dense QCD: Massive Yang-Mills approach at one-loop. Phys. Rev. D, 100(7):076017, 2019.
- [60] Romain Contant and Markus Q. Huber. Dense two-color QCD from Dyson-Schwinger equations. Phys. Rev. D, 101(1):014016, 2020.
- [61] T. G. Khunjua, K. G. Klimenko, and R. N. Zhokhov. The dual properties of chiral and isospin asymmetric dense quark matter formed of two-color quarks. JHEP, 06:148, 2020.
- [62] Toru Kojo and Daiki Suenaga. Thermal quarks and gluon propagators in two-color dense QCD. Phys. Rev. D, 103(9):094008, 2021.
- [63] Daiki Suenaga and Toru Kojo. Delineating chiral separation effect in two-color dense QCD. Phys. Rev. D, 104(3):034038, 2021.
- [64] Toru Kojo and Daiki Suenaga. Peaks of sound velocity in two color dense QCD: Quark saturation effects and semishort range correlations. Phys. Rev. D, 105(7):076001, 2022.
- [65] Daiki Suenaga, Kotaro Murakami, Etsuko Itou, and Kei Iida. Probing the hadron mass spectrum in dense two-color QCD with the linear sigma model. Phys. Rev. D, 107(5):054001, 2023.
- [66] M. Kobayashi and T. Maskawa. Chiral symmetry and eta-x mixing. Prog. Theor. Phys., 44:1422–1424, 1970.
- [67] M. Kobayashi, H. Kondo, and T. Maskawa. Symmetry breaking of the chiral $u(3) \times u(3)$ and the quark model. Prog. Theor. Phys., 45:1955–1959, 1971.
- [68] Gerard 't Hooft. Computation of the Quantum Effects Due to a Four-Dimensional Pseudoparticle. Phys. Rev. D, 14:3432–3450, 1976. [Erratum: Phys.Rev.D 18, 2199 (1978)].
- [69] Gerard 't Hooft. Symmetry Breaking Through Bell-Jackiw Anomalies. Phys. Rev. Lett., 37:8–11, 1976.
- [70] Kazuo Fujikawa. Path Integral Measure for Gauge Invariant Fermion Theories. Phys. Rev. Lett., 42:1195–1198, 1979.
- [71] T.P. Cheng and L.F. Li. Gauge Theory of Elementary Particle Physics. OUP Oxford, 1994.
- [72] H. Leutwyler and Andrei V. Smilga. Spectrum of Dirac operator and role of winding number in QCD. Phys. Rev. D, 46:5607–5632, 1992.
- [73] Max A. Metlitski and Ariel R. Zhitnitsky. Theta-parameter in 2 color QCD at finite baryon and isospin density. Nucl. Phys. B, 731:309–334, 2005.
- [74] Kotaro Murakami, Daiki Suenaga, Kei Iida, and Etsuko Itou. Measurement of hadron masses in 2-color finite density QCD. PoS, LATTICE2022:154, 2023.
- [75] G. Fejos and A. Hosaka. Thermal properties and evolution of the $U_A(1)$ factor for 2+1 flavors. Phys. Rev. D, 94(3):036005, 2016.
- [76] G. Fejós and A. Hosaka. Mesonic and nucleon fluctuation effects at finite baryon density. Phys. Rev. D, 95:116011, 2017.
- [77] G. Fejos and A. Hosaka. Axial anomaly and hadronic properties in a nuclear medium. Phys. Rev. D, 98(3):036009, 2018.

- [78] G. Fejös and A. Patkos. Backreaction of mesonic fluctuations on the axial anomaly at finite temperature. Phys. Rev. D, 105(9):096007, 2022.
- [79] Mark G. Alford, Andreas Schmitt, Krishna Rajagopal, and Thomas Schäfer. Color superconductivity in dense quark matter. Rev. Mod. Phys., 80:1455–1515, 2008.